An improved representation of aerosol wet removal by deep convection and impacts on simulated aerosol vertical profiles

Yunpeng Shan[1, #, *]

1 Department of Atmospheric Science, University of Wyoming, Laramie, WY 82071, USA

Xiaohong Liu[2, *], Lin Lin[2], Ziming Ke[2], and Zheng Lu[2]

2 Department of Atmospheric Sciences, Texas A&M University, College Station, TX 77843

* Corresponding authors: Yunpeng Shan (yunpengs@nevada.unr.edu); Xiaohong Liu (xiaohong.liu@tamu.edu)

Now at Brookhaven National Laboratory, Upton, NY, 11973

This article has been accepted for publication and undergone full peer review but has not been through the copyediting, typesetting, pagination and proofreading process, which may lead to differences between this version and the Version of Record. Please cite this article as doi: 10.1029/2020JD034173.

Key points:

- Aerosol wet removal by deep convective clouds significantly impacts global aerosol vertical profiles

- Explicit convective cloud microphysics in wet removal scheme reduces overestimation of black carbon and sea salt concentrations in upper troposphere.

- Parameterization of cloud-borne (activated) aerosol detrainment from convective to stratiform clouds is an important step in improving the model performance

Abstract

We introduce a physics-based aerosol wet removal scheme with unified treatments of aerosol transport and removal by convective clouds into the Community Atmosphere Model version 6 (CAM6). Since several important physical processes are still neglected or poorly represented in this new physics-based scheme, we develop secondary improvements to the parameterizations of aerosol activation, resuspension, and cloud-borne aerosol detrainment in this new scheme. Changes in the aerosol wet removal scheme cause tropospheric aerosol concentrations to decrease to different extents: compared to the control run, the new physics-based scheme significantly decreases aerosol burdens by up to 60% over the southern Pacific Ocean, whereas the secondary improvements mitigate the decreasing tendency. The burden changes also depend on aerosol chemical components: the sulfate mass decrease is compensated by secondary production, black carbon (BC) is effectively removed via increasing the hygroscopicity of particulate organic matter from 0 to 0.2, and dust shows the most spatially heterogeneous changes. Simulated aerosol profiles are evaluated against aircraft-based observations over the Pacific and Atlantic Oceans. The secondary-improved scheme reduces the overestimations of upper tropospheric BC and sea salt concentrations by a factor of 10 and 1,000, respectively, and reproduces the dependence of BC mass decrease rates on cloud types. Consideration of convective cloud-borne aerosol detrainment plays the most important role in enhancing the aerosol wet removal and decreasing the positive biases of tropospheric BC and sea salt concentrations. We also

summarize unresolved issues related to convective cloud genesis and microphysics, cloud-borne aerosol evolution, and BC and dust emissions.

1. Introduction

Atmospheric aerosols play a significant role in affecting climate since they can induce radiative forcing directly by reflecting and absorbing sunlight (Haywood and Boucher, 2000), and indirectly by affecting the warm cloud albedo and lifetime (Albrecht, 1989; Twomey, 1977). The response of cold cloud (i.e., mixed phase and solid phase clouds) radiative forcing to aerosol pollution is more complicated and uncertain (Fan et al., 2016; Rosenfeld et al., 2008). Therefore, global climate models (GCMs) have implemented explicit parameterizations to represent aerosols and their interactions with warm and cold clouds. A particularly important objective of aerosol-climate models is to correctly simulate the spatial distribution of aerosols, especially the vertical distribution, since the atmospheric radiation forcing, thermodynamics, and cloud development are sensitive to aerosol distribution (Ramanathan and Carmichael, 2008; Rosenfeld et al., 2008; Wilcox et al., 2016). Alternatively, clouds are effective in determining the aerosol budget and aerosol spatial distributions. For example, Dickerson et al., (1987) stressed that the transport of aerosol particles from the surface to 10 km altitude by a convective system takes only a few hours, whereas the large-scale motion flows may take several days to weeks. Moreover, the uplifted aerosols have a feedback effect on the development of mixed-phase convective clouds (Fan et al., 2018; Yin et al., 2005). Therefore, the cloud impacts on aerosols through transport and removal should be explicitly parameterized to accurately model the aerosol climate effects.

Substantial efforts have been made in developing and improving aerosol and cloud parameterization schemes in GCMs. However, GCMs still produce unsatisfactory simulations of aerosol vertical distributions over remote regions. For example, a systematic discrepancy between simulated and observed aerosol profiles is the overestimation of BC aerosol mass concentrations in the upper troposphere (UT) (Samset et al., 2014; Schwarz et al., 2013). Schwarz et al. (2010) illustrated that an insufficient wet removal rate may be associated with this discrepancy. Aerosol wet removal is divided into two classes: in-cloud wet removal and below-cloud wet removal. The former involves three processes: 1) the cloud system lifts aerosols upwards and activates them to be cloud-borne (i.e., activated) aerosols in cloud droplets; 2) collision-coalescence between cloud droplets generates precipitation and the settling precipitating particles (e.g., raindrop and snow crystal) remove cloud-borne aerosols from atmosphere; 3) not all cloud-borne aerosols are removed, and the remaining ones are resuspended to atmosphere via cloud particle evaporation. Below-cloud wet removal means that settling precipitation particles collect interstitial (not activated) aerosols in the air and remove them. Previous studies found that the in-cloud wet removal is more important in determining aerosol profiles and mass burdens than the below-cloud wet removal (Flossmann et al., 1985; Schwarz et al., 2010). Therefore, the improvements of aerosol wet removal parameterization usually focus on three important parameters of in-cloud aerosol wet removal: aerosol activation rate, aerosol removal efficiency (removed cloud-borne aerosol over total cloud-borne aerosol), and aerosol resuspension rate.

Based on cloud type, aerosol wet removals via precipitation are roughly categorized into two classes: stratiform cloud removal and convective cloud removal, while the later one includes removal in both shallow and deep convective clouds. The parameterization of aerosol wet removal in stratiform cloud is “explicit” because a detailed cloud microphysical scheme is used to parameterize stratiform process rates (e.g., water vapor condensing rate, precipitation generating rate and cloud water evaporating rate) and then applied to calculate three aerosol wet removal parameters for stratiform clouds. In contrast, the parameterization of aerosol wet removal in convective clouds is “empirical” because convective cloud schemes generally use empirical assumptions or prescribed tuning parameters to estimate cloud properties and the aerosol wet removal parameters in convective clouds (Tost et al., 2010). In principle, larger uncertainties are associated with convective cloud wet removal schemes since application of prescribed parameters may not represent reality in a satisfactory way.

The European Centre Hamburg Model version 5 coupled with the Hamburg Aerosol Module (ECHAM5-HAM) is among the few models that treat aerosol wet removal in convective clouds based on explicit microphysical processes. The ECHAM5-HAM involves additional aerosol modes for in-droplet and in-crystal aerosols in both stratiform and convective clouds (Croft et al., 2012; Hoose et al., 2008), which enables the model to predict the evolution of cloud-borne (activated) aerosols. Lohmann (2008)

and Zhang et al. (2005) developed a convective cloud microphysics scheme to parameterize convective cloud microphysical process rates in ECHAM5.

Wang et al. (2013; hereafter W13) developed an aerosol wet removal scheme that couples convective cloud schemes [i.e., Zhang and McFarlane (1995) deep convection scheme (hereafter ZM95) and Park and Bretherton (2009) shallow convection scheme] with the Modal Aerosol Module [MAM; Liu et al. (2012)] and implemented this scheme into the Community Atmosphere Model version 5 (CAM5). The W13 scheme has also been implemented in the DOE Energy Exascale Earth System Model version 1 [E3SMv1; Wang et al. (2020)] to couple the aerosol wet removal with deep convection. For the shallow convection part, the coupling was done with the Cloud Layers Unified By Binormals (CLUBB) scheme, which unifies the treatments of stratiform clouds and shallow convective clouds and is coupled with a stratiform cloud microphysics scheme. Song and Zhang (2011; hereafter SZ11) developed a convective cloud microphysics scheme, which was coupled with ZM95 in CAM5. This opens up possibilities to estimate aerosol wet removal rates in deep convections in an "explicit" way. However, the fusion of W13 and SZ11 has not been established.

In addition to the lack of comprehensive information from cloud parameterization treatment mentioned above, bias in aerosol wet removal is also associated with neglected or questionably parameterized aerosol changes related to cloud microphysics. For instance, the Wegener-Bergeron-Findeisen (WBF) process, converting cloud liquid

water to cloud ice and snow in mixed-phase clouds, efficiently resuspends the cloud-borne aerosols into the air during the cloud water evaporation (Qi et al., 2017). Therefore, we need to subtract resuspended cloud-borne aerosols via WBF from removed aerosol concentration. However, the current CAM6 model neglects this aerosol resuspension process and transfers the cloud-borne aerosols into the precipitation phase, which are then wet removed. Another questionable simplification lies in the aerosol resuspension by rain droplet evaporation. The realistic evaporation of rain droplets (i.e., raindrop shrinkage) does not necessarily release cloud-borne aerosols until liquid water is totally evaporated. However, the current schemes assume that rain droplets release aerosols immediately as they evaporate, suggesting that the model overestimates resuspension of aerosols via rainwater evaporation (Wang et al., 2020).

The objective of this study is to introduce a novel physics-based aerosol wet removal scheme by coupling the SZ11 convective cloud microphysical scheme with the sophisticated aerosol wet scavenging scheme developed by W13 in CAM6. As a result, the treatment of aerosol wet removal in convective clouds is as explicit as it is in stratiform clouds. Additionally, we further develop this scheme by improving parameterizations of cloud-borne aerosol evolution in both stratiform and convective clouds. The detailed improvements include: 1) adding the resuspension of cloud-borne aerosols by the WBF process, 2) refining the secondary aerosol activation (i.e., activation of aerosols entrained from environment into cloud body) rate, 3) improving

the representation of aerosol resuspension by rainwater evaporation, and 4) considering the detrainment of cloud-borne aerosols. The remainder of this article is organized as follows. Section 2 introduces the CAM6 aerosol wet removal scheme and our improvements. Section 3 examines the sensitivity of aerosol global distributions to our improvements. Section 4 evaluates simulated aerosol concentration profiles against aircraft measurements. Section 5 presents progress achieved in this study and provides insights for further scheme improvements. Section 6 summarizes the key findings and main conclusions.

2. Model description and simulation setup

In this study, we implement and improve the aerosol wet removal schemes in the Community Earth System Model Version 2 [CESM2; Danabasoglu et al. (2020)]. CESM2 is a comprehensive model considering the representation of a set of components (e.g., atmosphere, ocean, land, sea ice, and ice sheet) related to the earth system. CAM6 is the atmosphere component of CESM2 that includes diverse physical, chemical and dynamical processes in the atmosphere. The four-mode version of the Modal Aerosol Module [MAM4; Liu et al. (2016)] in CAM6 includes the Aitken, accumulated, coarse and primary carbon modes. Different aerosol species are internally mixed within an aerosol mode and externally mixed between modes. The aging of primary carbonaceous aerosols depends on the surface coating of sulfate that occurs as condensation of sulfuric acid gas H_2SO_4 (g) on the carbonaceous aerosol surface and coagulation with sulfate aerosol (Liu et al., 2005). The aging process changes

hydrophobic primary carbonaceous aerosols to be hydrophilic and transfers them into the accumulation mode (Liu et al., 2016). MAM4 also carries cloud-borne aerosols between time steps once the interstitial (unactivated) aerosols are activated into cloud droplets, but neglects their advection.

2.1 Aerosol wet removal in the standard CAM6 model

CAM6 uses the CLUBB scheme to unify the treatment of shallow convective clouds and stratiform clouds, which is also coupled with a two-moment cloud microphysics scheme (Gettelman and Morrison, 2015; Gettelman et al., 2015; hereafter as MG2). Cloud microphysical process rates predicted from MG2 are used in the stratiform (including shallow convection hereafter) aerosol wet removal scheme. As a result, the aerosol wet removal scheme for stratiform clouds can treat the activation of aerosols based on diagnosed in-cloud supersaturation, the removal of cloud-borne aerosols based on the precipitation efficiency from the cloud microphysics scheme, and the resuspension of cloud-borne aerosols based on rainwater and cloud water evaporation rates. In contrast, the deep convection scheme which is parameterized by the ZM95 scheme in CAM6 neglects detailed cloud microphysics and uses prescribed parameters to estimate deep convective cloud formation and precipitation. Therefore, the corresponding wet removal scheme uses empirical parameters to estimate aerosol activation, and removal and resuspension rates in deep convective clouds.

2.2 Scheme modifications and experiment setup

In this section, we discuss in detail our improvements to enable the aerosol wet removal scheme to better reflect the realistic physical nature of aerosol in-cloud wet removal.

We attempt to refine empirical parameterizations of aerosol activation, removal, and resuspension rates in deep convective clouds and construct a complete evolution of cloud-borne aerosols in the detrainment from convective clouds to stratiform clouds. Scheme improvements are summarized in Table 1 and details are described in the following sub-sections. Note that the current CAM6 model only considers wet removal of aerosols serving as cloud condensation nuclei (CCNs) and neglects wet removal of the ice nuclei particles (INPs). Therefore, our improvements only focus on the cloud microphysical processes related to warm and mixed-phase clouds.

2.2.1 Control experiment (CTL)

There are no changes involved with CTL and the default schemes are used. For aerosol wet removal in stratiform clouds, CAM6 predicts activated aerosol concentrations based on the Abdul-Razzak and Ghan (2000) parameterization and assumes that the loss rate of stratiform cloud-borne aerosols is proportional to the ratio of rainwater production rate calculated from the MG2 microphysics scheme to the total cloud hydrometer mass. The aerosol wet removal rate in deep convection is determined in the same fashion as aerosol wet removal in stratiform clouds except that prescribed parameters are used. In deep convective clouds, CTL prescribes the aerosol activation fractions to be 0.4, 0 and 0.8 for dust, BC/particulate organic matter (POM) and other aerosol species, respectively. In addition to the aerosol activation, CTL prescribes the cloud-borne aerosol removal efficiencies as 7.5×10^{-3} and 3×10^{-2} for the continental and marine convective clouds, respectively.

2.2.2 Physics-based scheme of aerosol wet removal in deep convective clouds (CONV)

CONV introduces a unified treatment of aerosol wet removal processes in deep convective clouds developed by W13, including: (1) simultaneous aerosol wet removal and transport, (2) explicit treatment of secondary aerosol activation, (3) specific assumption that wet removal only occurs in updrafts, and (4) entrainment and detrainment changing aerosol concentrations in the convective core. Additionally, CONV is expected to address the issue that the convective cloud precipitation rate used in the parameterization of convective aerosol wet removal is estimated with prescribed parameters, rather than explicit microphysical process rates. These prescribed parameters can neither physically represent the precipitation production nor reflect the warm cloud precipitation inhibition induced by aerosol pollution. Therefore, we couple SZ11, which provides a physics-based treatment of precipitation generation that involves auto-conversion, accretion and rimming, with W13 for an explicit aerosol wet removal rate. Also, CONV passes the convective updraft vertical velocity from SZ11 to the W13 scheme to calculate the Lagrangian time step length for a better estimation of total concentrations of removed aerosols (see more details in the supplement).

2.2.3 Further modifications of physics-based scheme (ToMod)

The combination of W13 and SZ11 introduces a physics-based scheme of aerosol wet removal in convective clouds which is as explicit as the aerosol wet removal scheme of stratiform clouds. However, CONV still neglects the detrainment of cloud-borne aerosols and cloud-borne aerosol resuspension due to the WBF process. Also, it employs a constant in-cloud supersaturation for the secondary aerosol activation and overestimates the aerosol resuspension due to rainwater evaporation. In this section, we

describe a scheme involving total further improvements to CONV (named as ToMod) to eliminate the aforementioned drawbacks in CONV. The details of our improvements are listed as follows and mathematical derivation is given in the supplement.

a. Aerosol resuspension by the WBF process (WBFR)

WBFR considers aerosol resuspension by the WBF process that serves as an effective approach to release cloud-borne aerosols back to the atmosphere. Qi et al. (2017) found that perturbation of BC concentration induced by WBF process can be as large as 150%. However, Qi et al. (2017) assumed that all hydrophilic BC particles are incorporated in the condensed phase and WBF-induced aerosol resuspension rate is exponentially related to temperature or solid cloud particle mass fraction (Cozic et al., 2007). These assumptions may introduce considerable biases because of the absences of accurately estimated WBF rate and cloud-borne aerosol concentrations. In this study, both the stratiform and deep convective cloud microphysics are fully coupled with the corresponding aerosol wet removal parameterizations, indicating that the wet removal module can calculate the cloud-borne aerosol concentrations and aerosol resuspension based on the WBF process rate provided by the cloud microphysics schemes. Therefore, we revisit the importance of WBF-induced aerosol resuspension for both stratiform and convective clouds in this study.

According to previous studies (Fan et al., 2011; Korolev, 2007), the WBF process occurs in the mixed-phase clouds where air is subsaturated with respect to liquid but still supersaturated with respect to ice. The loss of cloud liquid water mass induced by

evaporation during WBF is consistent with the "heterogeneous loss of mass" hypothesis that a portion of cloud droplets, no matter how large they are, immediately shrinks, while the remaining cloud droplets retain constant sizes (Beals et al., 2015). The phenomenon of smaller cloud droplets totally evaporating and larger droplets shrinking to smaller ones seldom occurs. Therefore, it is appropriate to assume that the aerosol mass increase caused by the WBF process is linearly proportional to the cloud liquid water evaporation rate. By assuming that cloud droplets are in mono-disperse size distributions, we parameterize the aerosol number increase rate by the WBF process to be proportional to the aerosol mass increase rate.

b. Secondary aerosol activation (SA)

Aerosols entrained from environments can be activated inside convective clouds, which is defined as the secondary aerosol activation. W13 attempted to parameterize the secondary aerosol activation at layers above convective cloud base using a constant supersaturation (i.e., 0.3%). However, previous observational studies found significantly varying, rather than constant, supersaturations existing in the convective clouds (Politovich and Cooper, 1988; Siebert and Shaw, 2017). Therefore, we pass the predicted convective updraft vertical velocities by SZ11 into the W13 scheme to calculate the in-cloud supersaturation and the aerosol activation rates (see supplement for more details). Consequently, the aerosol wet removal scheme can calculate the concentrations of activated aerosols in convective clouds.

c. Aerosol resuspension by rainwater entire evaporation (REE)

The aerosol wet removal scheme overestimates the occurring frequency of aerosol resuspension by rainwater evaporation since the current scheme assumes that aerosol release rate is proportional to the mass shrinking rate of evaporating raindrops. However, the physical nature is that rain droplets do not release aerosols until they completely evaporate. The parameterization of aerosol releasing rate by evaporating rainwater is different from the releasing rate by evaporating cloud water, because evaporating cloud droplets can only survive for a few seconds in an unsaturated environment (Bryan and Fritsch, 2002), which is much shorter than the model timestep (i.e., 5 minutes for stratiform cloud microphysics and 30 minutes for convective cloud microphysics), whereas large evaporating rain droplets can do it. The stratiform cloud microphysics scheme has a prognostic treatment of rainwater, allowing rain droplets to be carried over between model timesteps. Therefore, we calculate the aerosol resuspension determined by an "all-or-none" function judged by the occurrence of complete rainwater evaporation, following Wang et al. (2020).

Additionally, we consider the mode conversion of aerosols released by rain droplet evaporation. In warm clouds, the formation of a rain droplet (with a typical diameter of 2 mm) is through the collision and coalescence of one million cloud droplets (with the diameter of 20 μm). Note that one million cloud droplets contain the mass of one million cloud-borne aerosols serving as CCNs, indicating that one rain droplet contains the mass of one million aerosol particles. Therefore, the complete evaporation of this rain droplet will release a large aerosol particle whose mass is equal to the summation

of all CCN masses and should be released to the coarse aerosol mode. In this modification, dust, sea salt and sulfate aerosols released by the rain evaporation are redistributed to the corresponding coarse mode aerosols. Also, released POM, secondary organic aerosol (SOA) and BC mass are redistributed into the corresponding accumulated mode aerosol mass. Note that POM, SOA and BC, should also be redistributed into the coarse mode, but the coarse mode in current MAM4 does not have these aerosol species (i.e., SOA, POM and BC). The E3SMv1 by Wang et al. (2020) improved the MAM4 scheme that the coarse mode involves all aerosol species in the Atkin, primary carbon and accumulated modes. Such a progress is also expected by the CESM2 to facilitate the parameterization of evolution of aerosol released by evaporating raindrops.

d. Detrainment of convective cloud-borne aerosols (DR)

We convert convective cloud-borne aerosols into stratiform cloud-borne aerosols through the detrainment of convective cloud water to establish a representation of complete cloud-borne aerosol life cycle. In the ZM95 deep convection scheme, no cloud particles are carried over between timesteps. Three sink terms (i.e., evaporation, precipitation, and detrainment) are accounted by cloud water produced by condensation in convective clouds. The evolution of convective cloud-borne aerosols should be consistent with the convective cloud water, suggesting that convective cloud-borne aerosols should be removed through precipitation, resuspended through cloud water evaporation, and transferred into the stratiform clouds through detrainment of cloud water. However, previous studies [e.g., W13 and Yu et al. (2019)] neglected the

detrainment of cloud-borne aerosols and released all convective cloud-borne aerosols survived from precipitation removal to the atmosphere for simplification. Therefore, we enable the wet removal scheme to treat the detrainment of convective cloud-borne aerosols into stratiform clouds where they experience further removal by stratiform precipitation. Mass and number concentrations of detrained convective cloud droplets are added to the corresponding mass and number concentrations of stratiform cloud droplets, which causes the variation of stratiform cloud droplet size distribution.

2.3 Model configurations

We performed eight model experiments, as summarized in Table 1: the control experiment (CTL) with all the default setups, CONV combining W13 and SZ11, ToMod with all further changes to CONV, and sensitivity tests of each modifications in Section 2.2.3 (i.e., WBFR, SA, REE and DR). Liu and Wang (2010) stressed that the biomass burning emitted POMs are hydrophilic and have a hygroscopicity ranging from 0 to 0.3 while POMs from fossil and bio-fuel emissions are hydrophobic and have a hygroscopicity close to 0. However, the current MAM4 scheme treats all POMs as hydrophobic aerosols and sets the hygroscopicity of POMs (i.e., κ_{POM}) as 0, which significantly underestimates κ_{POM}. In this study, we increase the κ_{POM} from 0 to 0.2 in ToMod to achieve a κ_{POM} closer to physical nature and enable the deep convective clouds to effectively activate carbonaceous aerosols. We further investigate the model sensitivity to the change in κ_{POM} only. All the experiments, excluding CTL, turn on the SZ11 deep convective cloud microphysics scheme and the W13 convective aerosol removal scheme. In the main text, our analysis focuses on results from CTL, CONV

and ToMod, and importance of each physical process modifications are shown in Section 3 of the supplement. All experiments, with horizontal resolution of 0.9°×1.25° and 32 vertical levels, were run for 6-yr with the present-day (the year of 2000) aerosol and precursor gas emissions of the Coupled Model Intercomparison Project Phase 6 (CMIP6). The model timestep was 30 minutes. Results from the last 5-year simulations are used in our analysis.

3. Aerosol global distributions and mass budgets

We examine the responses to the wet removal changes of three aerosol species: sulfate, BC and dust, because they exhibit significantly varying and uncertain sensitivities to wet removal. Sulfate aerosols should be sensitive to the wet removal improvements because of its high hygroscopicity. However, aqueous-phase chemical reactions in cloud water produce secondary sulfate aerosols, which may compensate the wet removal of sulfate. Primary BC is hydrophobic but will become hydrophilic after coated by sulfate, which induces varying responses to wet removal improvements. Finally, when dust aerosols are transported from emission source to remote regions, the ratio of dust wet and dry deposition rates increases from 1 to 20 because of decreased coarse-mode dust burdens (Zhao et al., 2006; Zhao et al., 2003).

3.1 Global aerosol burden distribution

Sulfate aerosols have maximal concentrations over industrial regions like East Asia, Europe and North America (Fig. 1 A-C). The three simulations show similar geographic distributions of sulfate concentrations, whereas the relative differences are within ±20%

in the source regions (Fig. 1 D-F). We attribute the small mass perturbation to overwhelming secondary production by SO_2 aqueous-phase oxidation compensating the sulfate aerosol decrease by wet removal. Larger sulfate burden perturbations occur in the tropical regions where SO_2 concentrations are lower and precipitation is stronger. For example, Figure 1 D shows that CONV simulates tropical sulfate burdens that are 60% larger than CTL. Figure 1 E illustrates that the relative differences of sulfate mass burdens between ToMod and CTL in the tropical areas (ranging from 20% to 40%) is also positive but smaller than the corresponding differences between CONV and CTL. Overall, compared with CTL, CONV decreases the sulfate removal in the tropical regions and increases the sulfate removal in the high latitudes of the northern hemisphere (NH), and changes by ToMod are consistent with CONV but to a smaller extent. Increases in sulfate mass burdens in the high latitudes of the southern hemisphere in CONV and ToMod are a result of decreases in the sulfate removal there.

High BC concentrations occur in the midlatitude regions of the NH and low latitude regions over Southern Africa and Amazonian Rainforest which corresponds to industrial and biomass burning emissions, respectively. Outflow transport from the source regions is also seen in downstream regions (e.g., northern Pacific Ocean, tropical Atlantic Ocean and tropical Pacific Ocean; Fig. 2 A-C). CONV generally introduces a global decrease in BC burdens by up to 40 % with an exception that BC burden over the tropical oceanic regions (i.e., tropical warm pool and equatorial Atlantic Ocean; Fig. 2 D) slightly increases by 20 %. ToMod, however, decreases BC burdens over the globe

by 58 %, particularly over the oceanic regions compared with the differences between CTL and CONV simulations (Fig. 2E-F). The most significant burden decrease (i.e., larger than 80 %) is found over the central and southern Pacific Ocean. The BC mass burden in tropical region is less sensitive to scheme changes from CTL to CONV than sulfate since both CTL and CONV treat primary BC as hydrophobic aerosols, whereas sulfate aerosols are hydrophilic. BC simulated by ToMod is more sensitive to wet removal because of the increased κ_{POM}.

Dust aerosols concentrate over the source regions such as Northern Africa, Southwest and Central Asia, and outflow regions such as the western Pacific and the Atlantic Ocean (Fig. 3 A-C). Dust concentrations over source regions can be hundreds of times higher than those over the outflow oceanic regions, showing larger spatial concentration gradients than sulfate and BC. Dust mass burden changes in the source and outflow regions by CONV and ToMod are generally within 20% (Fig. 3 D-E), respectively, whereas dust burden decreases over the south Pacific Ocean by ToMod are larger than 80% (Fig. 3 D-E). Compared with CTL, CONV and ToMod introduce decreased concentrations of dust (i.e., aerosols mainly in the coarse mode) over the remote oceanic regions stronger than the concentration decreases of BC and sulfate (i.e., aerosols mainly in the accumulated mode). The main reason is that aerosol size matters more than chemical properties in determining the aerosol activation rate and the subsequent wet removal rate (Dusek et al., 2006). Relative difference between ToMod and CONV (Fig. 3 F) shows dust mass burden increases over high latitude regions where the mixed-

phase stratiform clouds are prevalent, which could be associated with the WBF process resuspending aerosols in the clouds.

3.2 Aerosol zonal mean distribution

In this section, vertical distributions of aerosols and their transport toward the Arctic regions are examined. Sulfate aerosols are emitted from anthropogenic activities at surface, lifted to UT layers by convection, and transported to the Arctic regions. During transport, secondary production by oxidation of sulfur dioxide significantly increases UT sulfate aerosol mass and compensates sulfate loss by dry and wet deposition. Stable stratification in the Arctic prevents local sulfate aerosols from reaching the free troposphere. The contributions of sulfate aerosols via long-range transport from the Northern Hemisphere midlatitudes vary with altitudes: long-range transport contributes to 90% of UT sulfate aerosol and to 50% of the planetary boundary layer (PBL) sulfate aerosol (Breider et al., 2014; Yang et al., 2018). The PBL sulfate aerosol concentration is close to UT sulfate aerosol concentration (Yang et al., 2018). In contrast, CTL shows that UT sulfate aerosol concentration is up to 200 ng/m^3 which is higher than PBL sulfate aerosol concentration that is up to 100 ng/m^3 (Fig. 4 A). By increasing UT aerosol wet removal rates with advanced parameterizations, CONV and ToMod decrease the UT sulfate aerosol concentration to be comparable with the PBL sulfate aerosol concentration, leading to a better simulation of sulfate aerosol profile in the Arctic.

BC aerosols have high concentrations over latitudes ranging from 30S to 60N, indicating that both anthropogenic emission in the midlatitude and biomass burning emission in the tropics predominantly contribute to the tropospheric BC aerosols and their subsequent transport toward the polar regions (Fig. 5 A-C). Wet removal should be more effective in changing the vertical distributions of BC than sulfate, because BC is primary aerosol and does not have in-cloud source to compensate the wet removal. Excluding the lower troposphere in the tropical regions, wet removal changes by CONV decrease the global BC concentrations by up to 60% compared to CTL (Fig. 5 D). Furthermore, when compared to CTL, the BC concentration reduction at UT introduced by ToMod are more than 80% (Fig. 5 E). This large UT BC reduction by ToMod is associated with the enlarged κ_{POM} which increases BC activation rates and consideration of convective cloud-borne aerosol detrainment that facilitates the further BC wet removal. As a result, BC aerosols advected to the Arctic concentrate in the PBL, whereas CONV and CTL show transported BC in the Arctic spreading throughout the tropospheric column (Fig. 5 A-C). Further evaluation in Section 4 verifies that ToMod successfully reproduces BC profiles in the polar regions, indicating that the changes by ToMod are reasonable.

Dust aerosols concentrate in the coarse mode, suggesting that due to their large size, they experience stronger gravitational settling toward the surface than BC and sulfate during the transport from middle latitude region to Arctic. Consequently, dust has the larger vertical mass decay rate than BC and sulfate. Previous studies [e.g., Liu et al.

(2012)] found that dust aerosols are transported toward the Arctic mainly in the UT layers. However, dust aerosol occurrence frequencies retrieved by CloudSat/Cloud‐Aerosol Lidar and Infrared Pathfinder Satellite Observations (CALIPSO) exhibits that Arctic dust usually occurs (mainly during spring) at 2 km to 6 km and seldom reaches 10 km (Luo et al., 2014). Therefore, increasing Arctic dust mass concentrations from 4 km to 10 km simulated by CTL may be questionable (Fig. 6 A). In contrast, CONV and ToMod decrease Arctic dust mass concentrations in the UT layers by 50 to 75% (Fig. 6 D - E). Wu et al. (2020) found that CESM2 underestimates the Arctic dust concentration and extinction by one order of magnitude and attributed this underestimation to small dust emissions in CESM2. Therefore, a follow-up study is expected to examine the response of dust vertical profiles to the aerosol wet removal parameterization after correcting the dust emissions.

4. Evaluations of vertical aerosol distributions against observations

We take BC and sea salt as examples to evaluate the impacts of aerosol wet removal scheme modifications on the simulations of aerosol vertical distributions. The observational datasets involve vertical distributions of BC aerosol across the Pacific measured by a Single-Particle Soot Photometer (SP2) during the High-Performance Instrumented Airborne Platform for Environmental Research (HIAPER) Pole-to-Pole Observations (HIPPO) campaigns [www.hiaper.ucar.edu; Schwarz et al. (2013); Schwarz et al. (2010)]. We also use BC aerosol mass mixing ratios (MMRs) measured by SP2 and sea salt concentrations measured by the Particle Analysis by Laser Mass

Spectrometry (PALMS) across the Pacific and Atlantic abroad NASA's DC-8 aircraft during the 2016-2018 Atmospheric Tomography (ATom) Mission [https://espo.nasa.gov/atom; Bian et al. (2019); Brock et al. (2019); Murphy et al. (2019)]. These global-scale datasets provide a large number of samplings of aerosol profiles extending from the PBL to ~12 km across a wide range of latitudes from 85S to 67N. Observed aerosol profiles are averaged in certain latitude-longitude ranges corresponding to the flight tracks. The sampling periods of HIPPO and ATom field campaigns cover five and four months corresponding to four seasons. Hence, averages of HIPPO and ATom samples can represent annual mean of BC and sea salt vertical distributions. Simulated aerosol profiles are from climatological means at locations and times closest to the aircraft flight tracks.

Our improvements mainly focus on the parameterizations of in-convective cloud wet removal, which motivates us to investigate the aerosol profiles in the regions dominated by convective clouds. Yang et al. (2015; see their Fig. 6) considered the convective storm updraft as a single plume and divided the aerosol profiles from the surface to 12 km into four vertical layers: a well-mixed layer (from surface to 3 km), a buffer layer (3-7km), a clean layer (7-9.5 km) and a tropopause layer (9.5-12 km). Aerosol concentrations at these four layers show distinct characteristics. From the well-mixed layer to the clean layer, the magnitude of aerosol MMR decreases with height, since the aerosols are generally lifted from the surface and removed in the convective core. Higher concentrations of aerosol at the tropopause layer are associated with the aerosols

released from the dissipation of convective anvils. The observed BC profiles in the tropical band (20S-20N) by HIPPO and ATom (Figs. 7 and 8 C) are similar to Yang et al. (2015) aerosol profiles: all these profiles show the BC mass mixing ratio decrease by one order of magnitude from 3 km to 6 km because of strong warm cloud and precipitation processes in the deep convection.

Model simulations show varying performances in reproducing the observed BC profiles in the tropics (e.g., Figs. 7 C and 8 C). CTL simulates BC MMR of $O(10^0)$ nearly constantly from the surface to 15 km, which overestimates BC MMR at the whole tropospheric layer. While the BC profile from the CONV simulation shows a weak BC MMR decreasing tendency with altitude which is closer to observation than CTL, it also fails to capture the correct BC decreasing trend. The ToMod simulation reproduces the observed BC profiles over the tropical Pacific Ocean (Fig. 7 C) and BC MMR at tropopause over the Atlantic Ocean (Fig. 8 C). An exception is that all simulations underestimate the BC MMR at the lower layers over the Atlantic (Fig. 8 C), which may be due to the emission inventory used in the simulation failing to capture the strong biomass burning events over central Africa. We attribute the improved model performance to the consideration of both convective cloud-borne aerosol detrainment and increased κ_{POM}, enabling the wet removal scheme to reflect the correct carbonaceous aerosol activation and removal rates.

The BC MMRs in the layers above 3 km over Arctic regions decrease slightly with altitude, while the BC MMRs over the Antarctic increase with altitude (see Fig. 7-8 A and E) indicating upper-level BC transport towards the Antarctic regions. Note that ATom and HIPPO show different BC MMRs from 9 km to 12 km over the Antarctic (Fig. 7 E) and from surface to 3 km over the Arctic (Fig. 7 A). Therefore, we emphasize the evaluation of model performances at those layers (i.e., surface to 9 km over the Antarctic and 3 km to 12 km over the Arctic) where BC MMRs observed by HIPPO and ATom are consistent. The evaluation shows that CTL generally overestimates BC MMR in both polar regions and fails to reproduce BC mass decreasing tendency with altitude over the Arctic, but simulates BC MMRs increasing with altitude. The improvement by CONV is very limited, because CONV, even though decreases the tropospheric BC MMRs, still simulates BC MMRs increasing with altitude. ToMod overperforms the CTL and CONV by reducing the overestimation of BC MMRs by 10 times at UT in the Arctic and capturing the Arctic BC MMRs decreasing with height at altitudes above 3 km. Sensitivity tests of parameterization modifications listed in Table 1 illustrate that ToMod eliminates the 10 times overestimation of UT BC MMRs in the polar regions because of 1) refined estimation of carbonaceous aerosol activation by increasing κ_{POM} and 2) consideration of convective cloud-borne aerosol detrainment both increase the BC wet removal.

Note that the simulated BC profiles over the NH midlatitudes by all three simulations fail to capture the observed BC MMR profile shape that BC MMRs increases with

height from surface to 6 km and then decreases with height at layers above 6 km (Fig. 7 and 8 B). We attribute the biases in simulation of aerosol profile shapes to the bias of BC emissions and especially complex aerosol-cloud interactions in this region. Previous studies [e.g., Liu et al. (2012)] stressed that the emission inventory of CESM, that stems from a technology-based global black carbon emission inventory developed by Bond et al. (2004) and Bond et al. (2007), underestimates the anthropogenic emissions in East Asia. The model uses of different years of emissions and meteorological conditions than the sampling years of field campaigns may also impact its comparison with the observations. Additionally, aerosol outflows from east Asia provide a large amount of CCN and INP that induce complex microphysical processes in the marine mixed-phase clouds. The limited capability of CESM2 in modeling evolutions of clouds and cloud-borne aerosols is also partially responsible for the failure in reproducing the BC profile shape.

In contrast, clouds over the latitude region 20S-60S usually have extraordinarily high liquid phase fraction because of low INP concentration (Huang et al., 2012a; Huang et al., 2012b). Additionally, BC aerosols over the Southern Ocean are usually from a unique source (i.e., biomass burning emissions). As a result, physical mechanisms related to the aerosol wet removal are not as diverse as the ones corresponding to NH midlatitude regions. Therefore, the scheme developments are efficient to improve the model performance, such as eliminating the 10-time overestimation of BC MMRs at the UT layer and capturing the correct BC MMR profile shape. Compared with CTL,

CONV simulates lower BC MMRs than CTL over the Pacific Ocean and Atlantic Ocean closer to observations (Fig. 7 and 8 D), but CONV still overestimates BC MMRs at layers higher than 6 km. ToMod successfully simulates the aerosol profiles with the best agreement with observations because of the increased carbonaceous aerosol activation and consideration of cloud-borne aerosol detrainment.

Note that sea salt aerosol mass concentrates in the coarse mode where the mean particle size is large. Additionally, hygroscopicity of sea salt aerosols is significantly higher than other types of aerosols. Therefore, both stratiform and convective clouds are able to generate supersaturation high enough to activate sea salt aerosols and lead their fate to wet removal. As a result, measured sea salt concentration profiles during the ATom field campaign (Figs. 9 and 10) in different sub-regions exhibit a unique character: strong decrease from $O(10^{-1})$ μg m^{-3} at 3 km to $O(10^{-5})$ μg m^{-3} at 12 km. The CTL overestimates sea salt concentrations at UT layers by two to three orders of magnitude. CONV decreases the overestimation to one to two orders of magnitude. Such an improvement by CONV benefits from the applications of the Abdul-Razzak and Ghan (2000) aerosol activation scheme capturing the correct sea salt activation efficiency and the physics-based parameterization of aerosol removal efficiency. Furthermore, ToMod eliminates the 1,000-time overestimation of sea salt concentrations at UT layers, which mainly benefits from the consideration of convective cloud-borne aerosol detrainment.

5. Discussion

As shown in previous studies [e.g., Schwarz et al. (2010)] and this study, one general bias in aerosol profile simulations is the overestimation of aerosol concentrations at UT layers (e.g., 10 times overestimation of BC and 1,000 times overestimation of sea salt) which is contributed to by underestimated aerosol wet removal in convective clouds. Note that CONV struggles to reduce the aerosol overestimations and keeps the 10 times overestimation of BC mass mixing ratio while it reduces the overestimation of sea salt concentrations to 10 to 100 times. ToMod further improves the model performance. Among all the scheme modifications in ToMod, DR and REE increase the aerosol wet removal, and WBFR decreases the aerosol wet removal. The contribution of SA is unclear because the predicted in-cloud supersaturation in deep convective clouds can be higher or lower than the prescribed value (i.e., 0.3%) by CONV. Our sensitivity tests show that DR is the most effective modification to decrease sea salt aerosol concentrations to agree with the observational magnitudes (Figs. S3-S4). For BC aerosols, both increasing κ_{POM} and DR are important in decreasing the 10 times overestimation of BC concentrations at UT (Figs. S1-S2). Other modifications (i.e., WBFR, REE and SA) do not significantly change the BC and sea salt aerosol concentrations (Figs. S1-S4). Therefore, we conclude that the progress in reducing the overestimations of BC concentrations (by 10 times) and sea salt concentrations (by 1,000 times) in UT existing in CTL is mainly attributed to increased aerosol convective wet removal through correctly estimating the aerosol activation rate and considering the convective cloud-borne aerosol detrainment. We achieved the correct aerosol

activation rate by increasing κ_{POM} to be closer to the observed values (see Subsection 2.3) and developed a complete cloud-borne aerosol evolution in the convective-cloud-stratiform-cloud system (see Subsection 2.2.3 d).

We highlight that further developments of the aerosol wet removal parameterization for deep convective clouds (i.e., ToMod) improve BC and sea salt aerosol vertical distributions over the globe, rather than only in the tropics. In particular, ToMod is successful in capturing the dependence of the BC profile shape on cloud types: the BC MMRs over stratiform-dominated regions (e.g., Arctic) slightly decrease with height at layers above 3 km, whereas the BC MMR profiles over convective-cloud-dominated regions (e.g., tropics) show sharp decreases at warm cloud layers (i.e., 3 km to 6 km). However, previous studies [e.g., W13 and Yu et al. (2019)] usually simulated BC concentrations over the Arctic regions increasing with altitude [see Fig. 6 in W13 and Fig. S1 in Yu et al. (2019)], even though they improved the simulation of BC profiles in the tropics. With improvements in capturing the magnitudes of UT BC and sea salt concentrations and reproducing these aerosol MMRs decreasing rates with altitude, CESM2 is able to represent at which vertical layer BC and sea salt survived from wet removal are advected from the emission regions to the remote regions. Based on more accurate estimation of BC and sea salt spatial distributions, follow-up studies can assess aerosol direct and indirect effects on climate by acting as CCN or light absorbing aerosols (Coopman et al., 2018a; Coopman et al., 2018b; Samset et al., 2013).

We also conduct sensitivity tests to investigate the relative importance of each individual processes listed in Section 2.2.3 (see Section 3 in supplement) and find that the simulation with cloud-borne aerosol detrainment is closest to ToMod. An explanation for the most important role of cloud-borne aerosol detrainment is that aerosols in convective clouds are efficiently activated, but only a very small fraction of them is removed via precipitation. Note that precipitation efficiency of convective clouds, even though known to be high, is generally lower than 50% (Fankhauser, 1988), suggesting that more than 50% of activated aerosols in deep convective clouds will survive from wet removal in convective clouds. Consequently, the treatment method of the evolution of these survived convective cloud-borne aerosols plays a substantial role in determining the aerosol concentrations. For the sake of simplification, previous studies (e.g., W13) neglected the cloud-borne aerosol detrainment and resuspended them locally, which leads to underestimated wet removal rates, whereas ToMod in this study detrains convective cloud-borne aerosols into stratiform clouds where they will experience further wet removal by the stratiform precipitation. To our knowledge, such a modification is the first attempt to establish the cloud-borne aerosol evolution in cumulus-to-stratiform detrainment, which is consistent with the cloud water evolution. For BC aerosols, we also need to increase κ_{POM} to activate more BC aerosols for the subsequent wet removal in convective clouds and stratiform clouds.

Here, we also discuss the uncertainties in the parameterizations of physical processes related to aerosol wet removal to guide future improvements. For the cloud component,

previous studies reported that the ZM95 scheme overestimates the convective cloud occurrence frequency (Boyle, 2005; Wang et al., 2009; Xie and Zhang, 2000), which may contribute to the slight underestimation of sea salt concentrations in the tropical regions (e.g., Fig. 9 C). Additionally, we need to accurately partition the deep convective cloud condensates into the sedimented and detained portions by improving the parameterizations of precipitating particle fall speeds and convective updraft vertical velocity (Lin et al., 2021). Moreover, we need to replace the double-moment treatment of rain droplet size distribution with a triple-moment one to eliminate the overestimation of drizzle rainfall rate and the underestimation of heavy rainfall rate (Shan, 2018; Shan et al., 2020).

For the aerosol component, the current scheme has represented the evolution of convective cloud-borne aerosols to be consistent with the evolution of convective cloud water, but still neglects the cloud-borne aerosol advection in stratiform clouds (Ghan and Easter, 2006). This assumption contradicts the treatment of cloud water advection in the model. We note that ToMod significantly improves the BC profiles over the remote regions away from strong BC sources, but still underestimates BC MMRs over the aerosol outflowing regions (e.g., 20N-60N in NH). Therefore, the further progress in simulating the BC spatial distributions relies on the precondition that the BC emission inventory is also improved. For the same reason, simulated dust profiles will be improved once CESM2 eliminates the dust concentration underestimation by one order of magnitude due to low dust emissions. Note that increasing the κ_{POM} in this

study compensates for the lack of redistribution of POM, SOA and BC into the coarse mode. We may need to further reduce the κ_{POM} to a lower value after implementation of POM, SOA and BC redistributions to the coarse mode.

6. Conclusions

In this study, we improved the treatment of cloud-borne aerosol evolution by refining the representation of microphysical processes in aerosol wet removal schemes for convective and stratiform clouds, with the main objective being to improve the simulations of aerosol vertical distributions. We analyzed the aerosol spatial distributions to understand the role of parameterization modifications. The model performance is evaluated against the aircraft-observed BC and sea salt aerosol mass profiles covering global latitudes ranging from the Arctic, tropics and to the Antarctic. Our scheme improvements are based on the NCAR CAM6 model, but it can be implemented in other global-scale and regional-scale chemistry-climate models.

Consistent with previous studies (Schwarz et al., 2010), the default CAM6 also displays positive biases in the UT aerosol concentrations (e.g., by a factor of 10 for BC and 1,000 for sea salt), which is speculated to be due to the underestimation of aerosol in-cloud wet removal. Our aerosol wet removal scheme for deep convective clouds (CONV), considering the physics-based parameterizations of aerosol activation and subsequent removal via precipitation, is not sufficiently efficient to improve simulated aerosol profiles. In this study, CONV decreases the sea salt concentration overestimation to a

factor of 100. However, BC MMRs at UT layers over the Arctic and tropical regions are still overestimated by a factor of 10. We further developed the CONV scheme by treating the aerosol resuspension from WBF and rainwater evaporation and improving parameterizations of secondary aerosol activation and convective cloud-borne aerosol evolution consistent with the detrainment of convective clouds to stratiform clouds. The further developed scheme (ToMod) successfully removes the overestimation of UT BC and sea salt concentrations by a factor of 10 and 1,000, respectively, and corrects the bias in the Arctic that modeled BC MMRs increase with altitude. Furthermore, ToMod shows a unique advantage in simultaneously capturing the three features of observations: sea salt concentrations decrease dramatically with altitude by 4 to 5 orders of magnitude from surface to the tropopause, tropical BC profiles exhibit a sharp decrease at warm cloud layers, and the Arctic BC profiles exhibit a weak mass decrease rate at layers above 3 km.

The aerosol wet removal scheme modifications also play a key role in changing the aerosol zonal distributions and mass burdens, where the new schemes (CONV and ToMod) introduce magnitude changes in aerosol concentrations (see Figs. 1-6 and Figs. S5-S6). Compared with aerosols over the source regions, aerosols over the outflow regions and at UT layers are more sensitive to the wet removal scheme changes. The relative differences of simulated aerosol concentrations by CTL from those by CONV and ToMod depend on the aerosol components but still exhibit consistent tendencies that the tropospheric aerosol concentrations simulated by CONV are ~40% lower than

those simulated by CTL. With the exception of BC, the zonal mean aerosol concentration changes by ToMod are consistent with CONV, but only accounts for up to 76% of CONV changes. ToMod eliminates the tenfold overestimation of BC MMRs and the 1000 times overestimation of sea salt concentrations at UT, indicating that ToMod is successful in capturing the global aerosol zonal mean distributions and mass burdens. Additionally, CESM2 with such an improved aerosol wet removal scheme is generally able to reproduce the aerosol transport path towards the remote regions (e.g., Arctic and tropics).

Acknowledgements. This work was funded by NASA CloudSat and CALIPSO Science Program (Grant Number: 80NSSC20K0952) and U.S. Department of Energy (DOE) Atmospheric System Research (ASR) Program (Office of Science, OBER) under Grant #DE-SC0018190. We wish to thank Cenlin He (NCAR), Hrongrong Shi (Chinese Academy of Sciences), Lei Zhang (Chinese Academy of Meteorological Sciences), Hunter Brown (University of Agricultural and Mechanical University), Lijuan Miao (Nanjing University of Information Science and Technology) and Meng Gao (Hong Kong Baptist University) for their fruitful discussion which significantly improves the original manuscript. We also appreciate Po-Lun Ma (PNNL), Lan Gao (University of Oklahoma), Joshua Schwarz (NOAA) and Kang Yang (University of Colorado, Boulder) for providing developed observational data. Authors would like to acknowledge the use of computational resources (doi:10.5065/D6RX99HX) at the NCAR - Wyoming Supercomputing Center provided by the National Science

Foundation and the State of Wyoming and supported by NCAR's Computational and Information Systems Laboratory. We would like to thank the reviewers for their constructive comments to help improve the manuscript. The High-Performance Instrumented Airborne Platform for Environmental Research (HIAPER) Pole-to-Pole Observations (HIPPO) campaigns observational dataset used in this study is available from the NASA EOL website https://www.eol.ucar.edu/field_projects/hippo. Atmospheric Tomography (ATom) Mission data can be download from website https://espo.nasa.gov/atom/content/ATom. The CAM6 simulation outputs for this study are available online (https:/doi.org/10.5281/zenodo.4818537).

References:

Abdul-Razzak, H., and S. J. Ghan (2000), A parameterization of aerosol activation: 2. Multiple aerosol types, *Journal of Geophysical Research: Atmospheres*, *105*(D5), 6837-6844, doi:10.1029/1999jd901161.

Albrecht, B. A. (1989), Aerosols, Cloud Microphysics, and Fractional Cloudiness, *science*, *245*, 1227-1230.

Beals, M. J., J. P. Fugal, R. A. Shaw, J. Lu, S. M. Spuler, and J. L. Stith (2015), Holographic Measurementss of Inhomogeneous cloud Mixing at the Centimenter Scale, *Science*, *350*(6256), 87-90.

Bian, H., et al. (2019), Observationally constrained analysis of sea salt aerosol in the marine atmosphere, *Atmospheric Chemistry and Physics*, *19*(16), 10773-10785, doi:10.5194/acp-19-10773-2019.

Bond, T. C., E. Bhardwaj, R. Dong, R. Jogani, S. Jung, C. Roden, D. G. Streets, and N. M. Trautmann (2007), Historical emissions of black and organic carbon aerosol from energy-related combustion, 1850-2000, *Global Biogeochemical Cycles*, *21*(2), n/a-n/a, doi:10.1029/2006gb002840.

Bond, T. C., D. G. Streets, K. F. Yarber, S. M. Nelson, J.-H. Woo, and Z. Klimont (2004), A technology-based global inventory of black and organic carbon emissions from combustion, *Journal of Geophysical Research*, *109*(D14), doi:10.1029/2003jd003697.

Boyle, J. S. (2005), Diagnosis of Community Atmospheric Model 2 (CAM2) in numerical weather forecast configuration at Atmospheric Radiation Measurement sites, *Journal of Geophysical Research*, *110*(D15), doi:10.1029/2004jd005042.

Breider, T. J., L. J. Mickley, D. J. Jacob, Q. Wang, J. A. Fisher, R. Y. W. Chang, and B. Alexander (2014), Annual distributions and sources of Arctic aerosol components, aerosol optical depth, and aerosol absorption, *Journal of Geophysical Research: Atmospheres*, *119*(7), 4107-4124, doi:10.1002/2013jd020996.

Brock, C. A., et al. (2019), Aerosol size distributions during the Atmospheric Tomography Mission (ATom): methods, uncertainties, and data products, *Atmospheric Measurement Techniques*, *12*(6), 3081-3099, doi:10.5194/amt-12-3081-2019.

Bryan, G. H., and J. M. Fritsch (2002), A benchmark simulation for moist nonhygrostatic numerical models, *Monthly Weather Review*, *130*, 2917-2928.

Coopman, Q., T. J. Garrett, D. P. Finch, and J. Riedi (2018a), High Sensitivity of Arctic Liquid Clouds to Long-Range Anthropogenic Aerosol Transport, *Geophysical Research Letters*, *45*(1), 372-381, doi:10.1002/2017gl075795.

Coopman, Q., J. Riedi, D. P. Finch, and T. J. Garrett (2018b), Evidence for Changes in Arctic Cloud Phase Due to Long-Range Pollution Transport, *Geophysical Research Letters*, *45*(19), 10,709-710,718, doi:10.1029/2018gl079873.

Cozic, J., B. Verheggen, S. Mertes, P. Connolly, K. Bower, A. Petzold, U. Baltensperger, and E.Weingartner (2007), Scavenging of black carbon in mixed phase clouds at the high alpine site Jungfraujoch, *Atmospheric Chemistry and Physics*, *7*, 1797-1807.

Croft, B., J. R. Pierce, R. V. Martin, C. Hoose, and U. Lohmann (2012), Uncertainty associated with convective wet removal of entrained aerosols in a global climate model, *Atmospheric Chemistry and Physics*, *12*(22), 10725-10748, doi:10.5194/acp-12-10725-2012.

Danabasoglu, G., et al. (2020), The Community Earth System Model Version 2 (CESM2), *Journal of Advances in Modeling Earth Systems*, *12*(2), doi:10.1029/2019ms001916.

Dickerson, R. R., et al. (1987), Thunderstorms: An Important Mechanism in the Transport of Air Pollutants, *Science*, *235*, 460-465.

Dusek, U., et al. (2006), Size Matters More Than Chemistry for Cloud-Nucleating, *Science*, *312*, 1375-1378.

Fan, J., S. Ghan, M. Ovchinnikov, X. Liu, P. J. Rasch, and A. Korolev (2011), Representation of Arctic mixed-phase clouds and the Wegener-Bergeron-Findeisen process in climate models: Perspectives from a cloud-resolving study, *Journal of Geophysical Research*, *116*, doi:10.1029/2010jd015375.

Fan, J., et al. (2018), Substantial convection and precipitation enhancements by ultrafine aerosol particles, *Science*, *359*, 1-8.

Fan, J., Y. Wang, D. Rosenfeld, and X. Liu (2016), Review of Aerosol-Cloud Interactions: Mechanisms, Significance and Challenges, *Journal of the Atmospheric Sciences*, *73*(4221-4252), doi:10.1175/JAS-D-16-0037.1.

Fankhauser, J. C. (1988), Estimates of thunderstorm precipitation efficiency from field mesaurements in CCOPE, *Monthly Weather Review*, *116*, 663-684.

Flossmann, A. I., W. D. Hall, and H. R. Pruppacher (1985), A Theoretical Study of the Wet Removal of Atmospheric Pollutants. Part I: The Redistribution of Aerosol Particles Captured through Nucleation and Impaction Scavenging by Growing Cloud Drops, *Journal of the Atmospheric Sciences*, *42*(6), 583-606.

Gettelman, A., and H. Morrison (2015), Advanced Two-Moment Bulk Microphysics for Global Models. Part I: Off-Line Tests and Comparison with Other Schemes, *Journal of Climate*, *28*(3), 1268-1287, doi:10.1175/jcli-d-14-00102.1.

Gettelman, A., H. Morrison, S. Santos, and P. Bogenschutz (2015), Advanced Two-Moment Bulk Microphysics for Global Models Part II: Global Model Solutions and Aerosol–Cloud Interactions, *Journal of Climate*, *28*, 1288-1307, doi:10.1175/JCLI-D-14-00103.s110.1175/JCLI-D-14-00103.1.

Ghan, S. J., and R. C. Easter (2006), Impact of cloud-borne aerosol representation on aerosol direct and indirect effects, *Atmospheric Chemistry and Physics*, *6*, 4163–4174.

Haywood, J., and O. Boucher (2000), Estimates of the direct and indirect radiative forcing due to tropospheric aerosols: A review, *Reviews of Geophysics*, *38*(4), 513-543, doi:10.1029/1999rg000078.

Hoose, C., U. Lohmann, P. Stier, B. Verheggen, and E. Weingartner (2008), Aerosol processing in mixed-phase clouds in ECHAM5-HAM: Model description and comparison to observations, *Journal of Geophysical Research*, *113*(D7), doi:10.1029/2007jd009251.

Huang, Y., S. T. Siems, M. J. Manton, L. B. Hande, and J. M. Haynes (2012a), The Structure of Low-Altitude Clouds over the Southern Ocean as Seen by CloudSat, *Journal of Climate*, *25*(7), 2535-2546, doi:10.1175/jcli-d-11-00131.1.

Huang, Y., S. T. Siems, M. J. Manton, A. Protat, and J. Delanoë (2012b), A study on the low-altitude clouds over the Southern Ocean using the DARDAR-MASK, *Journal of Geophysical Research: Atmospheres*, *117*(D18), n/a-n/a, doi:10.1029/2012jd017800.

Korolev, A. (2007), Limitations of the Wegener–Bergeron–Findeisen Mechanism in the Evolution of Mixed-Phase Clouds, *Journal of the Atmospheric Sciences*, *64*(9), 3372-3375, doi:10.1175/jas4035.1.

Lin, L., Q. Fu, X. Liu, Y. Shan, S. E. Giangrande, G. S. Elsaesser, K. Yang, and D. Wang (2021), Improved Convective Ice Microphysics Parameterization in the NCAR CAM Model, *Journal of Geophysical Research: Atmospheres*, *126*(9), doi:10.1029/2020jd034157.

Liu, X., et al. (2012), Toward a Minimal Representation of Aerosols in Climate Models: Description and Evaluation in the Community Atmosphere Model CAM5, *Geoscientific Model Development*, *5*(3), 709-739.

Liu, X., P. L. Ma, H. Wang, S. Tilmes, B. Singh, R. C. Easter, S. J. Ghan, and P. J. Rasch (2016), Description and evaluation of a new four-mode version of the Modal Aerosol Module (MAM4) within version 5.3 of the Community Atmosphere Model, *Geoscientific Model Development*, *9*(2), 505-522, doi:10.5194/gmd-9-505-2016.

Liu, X., J. E. Penner, and M. Herzog (2005), Global modeling of aerosol dynamics: Model description, evaluation, and interactions between sulfate and nonsulfate aerosols, *Journal of Geophysical Research*, *110*(D18), doi:10.1029/2004jd005674.

Liu, X., and J. Wang (2010), How important is organic aerosol hygroscopicity to aerosol indirect forcing?, *Environmental Research Letters*, *5*(4), 044010, doi:10.1088/1748-9326/5/4/044010.

Lohmann, U. (2008), Global anthropogenic aerosol effects on convective clouds in ECHAM5-HAM, *Atmospheric Chemistry and Physics*, *8*, 2115-2131.

Luo, T., Z. Wang, D. Zhang, X. Liu, Y. Wang, and R. Yuan (2014), Global dust distribution from improved thin dust layer detection using A-train satellite lidar observations, *Geophysical Research Letters*, 42, 620–642, 628, doi:10.1002/.

Murphy, D. M., et al. (2019), The distribution of sea-salt aerosol in the global troposphere, *Atmospheric Chemistry and Physics*, *19*(6), 4093-4104, doi:10.5194/acp-19-4093-2019.

Park, S., and C. S. Bretherton (2009), The University of Washington Shallow Convection and Moist Turbulence Schemes and Their Impact on Climate Simulations with the Community Atmosphere Model, *Journal of Climate*, *22*(12), 3449-3469, doi:10.1175/2008jcli2557.1.

Politovich, M. K., and W. A. Cooper (1988), Variablity of the Supersaturation in Cumulus Clouds, *Journal of the Atmospheric Sciences*, *45*(11), 1651-1664.

Qi, L., Q. Li, C. He, X. Wang, and J. Huang (2017), Effects of the Wegener–Bergeron–Findeisen process on global black carbon distribution, *Atmospheric Chemistry and Physics*, *17*(12), 7459-7479, doi:10.5194/acp-17-7459-2017.

Ramanathan, V., and G. Carmichael (2008), Global and regional climate changes due to black carbon, *Nature*, *1*, 221-227.

Rosenfeld, D., U. Lohmann, G. B. Raga, C. D. O'Dowd, M. Kulmala, S. Fuzzi, A. Reissell, and M. O. Andreae (2008), Flood or drought: how do aerosols affect precipitation?, *Science*, *321*(5894), 1309-1313, doi:10.1126/science.1160606.

Samset, B. H., et al. (2014), Modelled black carbon radiative forcing and atmospheric lifetime in AeroCom Phase II constrained by aircraft observations, *Atmospheric Chemistry and Physics*, *14*(22), 12465-12477, doi:10.5194/acp-14-12465-2014.

Samset, B. H., et al. (2013), Black carbon vertical profiles strongly affect its radiative forcing uncertainty, *Atmospheric Chemistry and Physics*, *13*(5), 2423-2434, doi:10.5194/acp-13-2423-2013.

Schwarz, J. P., B. H. Samset, A. E. Perring, J. R. Spackman, R. S. Gao, P. Stier, M. Schulz, F. L. Moore, E. A. Ray, and D. W. Fahey (2013), Global-scale seasonally

resolved black carbon vertical profiles over the Pacific, *Geophysical Research Letters*, *40*(20), 5542-5547, doi:10.1002/2013GL057775.

Schwarz, J. P., J. R. Spackman, R. S. Gao, L. A. Watts, P. Stier, M. Schulz, S. M. Davis, S. C. Wofsy, and D. W. Fahey (2010), Global-scale black carbon profiles observed in the remote atmosphere and compared to models, *Geophysical Research Letters*, *37*(18), n/a-n/a, doi:10.1029/2010gl044372.

Shan, Y. (2018), Evaluating and Improving the Multi-Moment Cloud Microphysics Scheme *PhD Thesis*, University of Nevada, Reno.

Shan, Y., E. M. Wilcox, L. Gao, L. Lin, D. L. Mitchell, Y. Yin, T. Zhao, L. Zhang, H. Shi, and M. Gao (2020), Evaluating Errors in Gamma-Function Representations of the Raindrop Size Distribution: A Method for Determining the Optimal Parameter Set for Use in Bulk Microphysics Schemes, *Journal of the Atmospheric Sciences*, *77*(2), 513-529, doi:10.1175/jas-d-18-0259.1.

Siebert, H., and R. A. Shaw (2017), Supersaturation Fluctuations during the Early Stage of Cumulus Formation, *Journal of the Atmospheric Sciences*, *74*(4), 975-988, doi:10.1175/jas-d-16-0115.1.

Song, X., and G. J. Zhang (2011), Microphysics parameterization for convective clouds in a global climate model: Description and single-column model tests, *Journal of Geophysical Research*, *116*(D2), doi:10.1029/2010jd014833.

Tost, H., M. G. Lawrence, C. Br¨uhl, P. J¨ockel, T. G. Team, and T. S.-O.-D. A. Team (2010), Uncertainties in atmospheric chemistry modelling due to convection

parameterisations and subsequent scavenging, *Atmospheric Chemistry and Physics*, *10*, 1931–1951.

Twomey, S. (1977), The Influence of Pollusion on the Shortwave Albedo of Clouds, *Journal of the Atmospheric Sciences*, *34*, 1149-1152.

Wang, H., R. C. Easter, P. J. Rasch, M. Wang, X. Liu, S. J. Ghan, Y. Qian, J. H. Yoon, P. L. Ma, and V. Vinoj (2013), Sensitivity of remote aerosol distributions to representation of cloud–aerosol interactions in a global climate model, *Geoscientific Model Development*, *6*(3), 765-782, doi:10.5194/gmd-6-765-2013.

Wang, H., et al. (2020), Aerosols in the E3SM Version 1: New Developments and Their Impacts on Radiative Forcing, *Journal of Advances in Modeling Earth Systems*, *12*(1), doi:10.1029/2019ms001851.

Wang, W., X. Liu, S. Xie, J. Boyle, and S. A. McFarlane (2009), Testing ice microphysics parameterizations in the NCAR Community Atmospheric Model Version 3 using Tropical Warm Pool–International Cloud Experiment data, *Journal of Geophysical Research*, *114*(D14), doi:10.1029/2008jd011220.

Wilcox, E. M., R. M. Thomas, P. S. Praveen, K. Pistone, F. A. Bender, and V. Ramanathan (2016), Black carbon solar absorption suppresses turbulence in the atmospheric boundary layer, *Proceedings of the National Academy of Sciences of the United States of America*, *113*(42), 11794-11799, doi:10.1073/pnas.1525746113.

Wu, M., et al. (2020), Understanding processes that control dust spatial distributions with global climate models and satellite observations, *Atmospheric Chemistry and Physics*, *20*(22), 13835-13855, doi:10.5194/acp-20-13835-2020.

Xie, S., and M. Zhang (2000), Impact of the convection triggering function on single-column model simulations, *Journal of Geophysical Research: Atmospheres*, *105*(D11), 14983-14996, doi:10.1029/2000jd900170.

Yang, Q., et al. (2015), Aerosol transport and wet scavenging in deep convective clouds: A case study and model evaluation using a multiple passive tracer analysis approach, *Journal of Geophysical Research: Atmospheres*, *120*, 8448–8468, doi:10.1002/.

Yang, Y., H. Wang, S. J. Smith, R. C. Easter, and P. J. Rasch (2018), Sulfate Aerosol in the Arctic: Source Attribution and Radiative Forcing, *Journal of Geophysical Research: Atmospheres*, *123*, 1899–1918, doi:10.1002/2017JD027298.

Yin, Y., K. S. Carslaw, and G. Feingold (2005), Vertical transport and processing of aerosols in a mixed-phase convective cloud and the feedback on cloud development, *Quarterly Journal of the Royal Meteorological Society*, *131*(605), 221-245, doi:10.1256/qj.03.186.

Yu, P., et al. (2019), Efficient In-Cloud Removal of Aerosols by Deep Convection, *Geophysical Research Letters*, *46*, 1061–1069, doi:10.1029/.

Zhang, G. J., and N. A. McFarlane (1995), Sensitivity of climate simulations to the parameterization of cumulus convection in the Canadian climate centre general circulation model, *Atmosphere-Ocean*, *33*(3), 407-446, doi:10.1080/07055900.1995.9649539.

Zhang, J., U. Lohmann, and P. Stier (2005), A microphysical parameterization for convective clouds in the ECHAM5 climate model: Single-column model results

evaluated at the Oklahoma Atmospheric Radiation Measurement Program site, *Journal of Geophysical Research*, *110*(D15), doi:10.1029/2004jd005128.

Zhao, T. L., S. L. Gong, X. Y. Zhang, J. P. Blanchet, I. G. McKendry, and Z. J. Zhou (2006), A Simulated Climatology of Asian Dust Aerosol and Its Trans-Pacific Transport. Part I: Mean Climate and Validation, *Journal of Climate*, *19*(1), 88-103, doi:10.1175/jcli3605.1.

Zhao, T. L., S. L. Gong, X. Y. Zhang, and I. G. McKendry (2003), Modeled size-segregated wet and dry deposition budgets of soil dust aerosol during ACE-Asia 2001: Implications for trans-Pacific transport, *Journal of Geophysical Research*, *108*(D23), doi:10.1029/2002jd003363.

Zipser, E. J., and M. A. Lemone (1980), Cumulonimbus Vertical Velocity Events in GATE. Part II: Synthesis and Model Core Structure, *Journal of Atmospheric Science*, 37(2458-2469)

Table 1. Summary of code changes in the current CAM6 model. The abbreviations (i.e., WBFR, REE, SA and DR), corresponding to the physical process modifications in Section 2.2.3, denote aerosol resuspension by WBF process, aerosol secondary activation, aerosol resuspension by rainwater entire evaporation and cloud-borne aerosol detrainment, respectively. "X" denotes that the modifications have been made to the treatments of the corresponding physical process or new treatments have been added to the scheme (see text for more details). "-" means that default setup is used while blank indicates the process is not considered. We also turn on/off the W13 and SZ11 scheme (see text for more details). κ_{POM} denotes sensitivity experiment for the hygroscopicity of POM.

	Scheme changes								
	κ_{POM}	Stratiform		Convective cloud					
		WBFR	REE	WBFR	REE	SA	DR	W13	SZ11
CTL	0		-		-			Off	Off
CONV	0		-		-	-		On	On
κ_{POM}_ST	0.2		-		-	-		On	On
WBFR_ST	0.2	X	-	X	-	-		On	On
REE_ST	0.2		X		X	-		On	On
SA_ST	0.2		-		-	X		On	On
DR_ST	0.2		-		-	-	X	On	On
ToMod	0.2	X	X	X	X	X	X	On	On

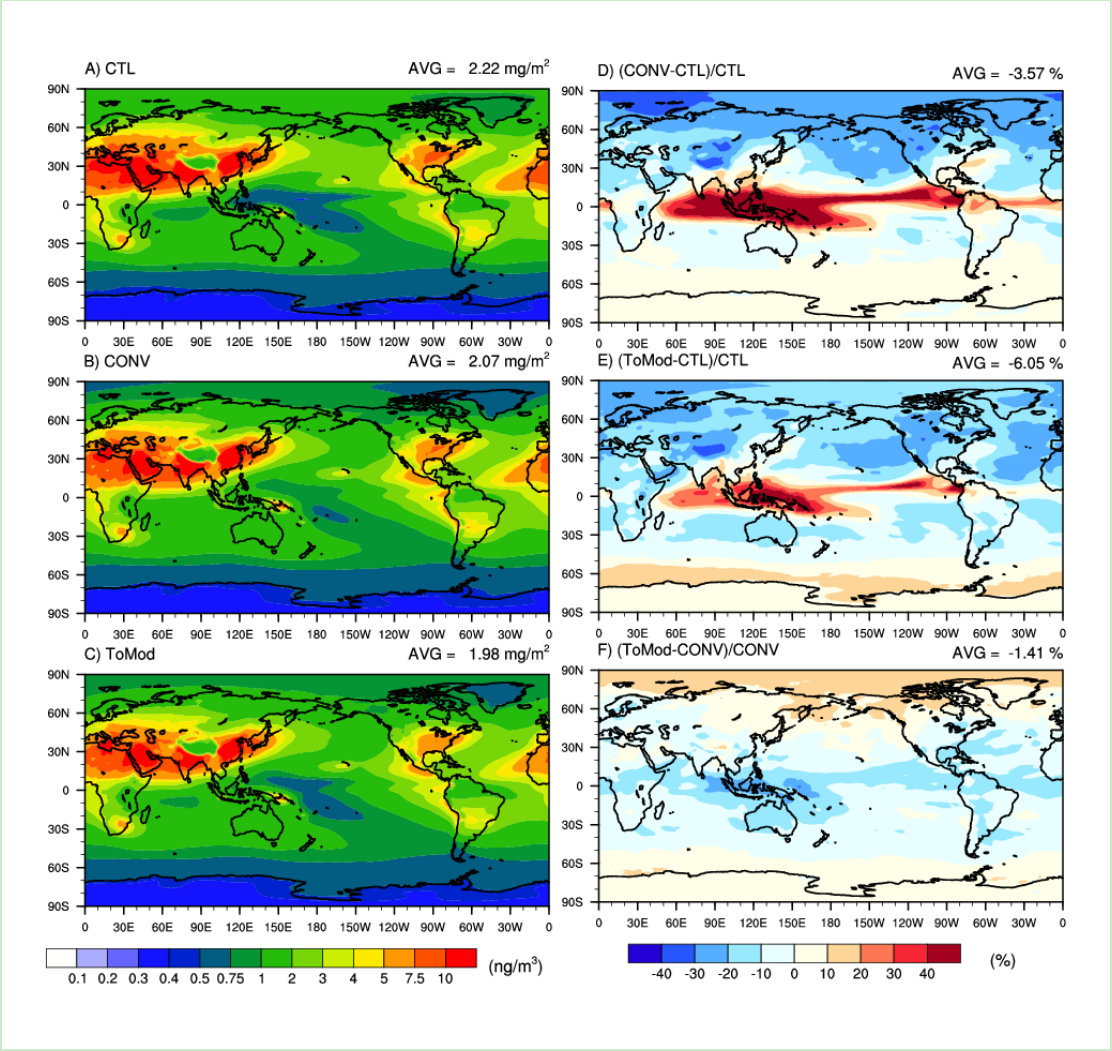

Fig. 1. The geographic distribution of the annual mean vertically integrated mass burdens of sulfate aerosols for simulations CTL (a), CONV (b) and ToMod (c) and the relative differences between CTL and CONV (d), CTL and ToMod (e) and CONV and ToMod (f). The acronyms are described in Table 1. The numbers on the panels denote the global averages.

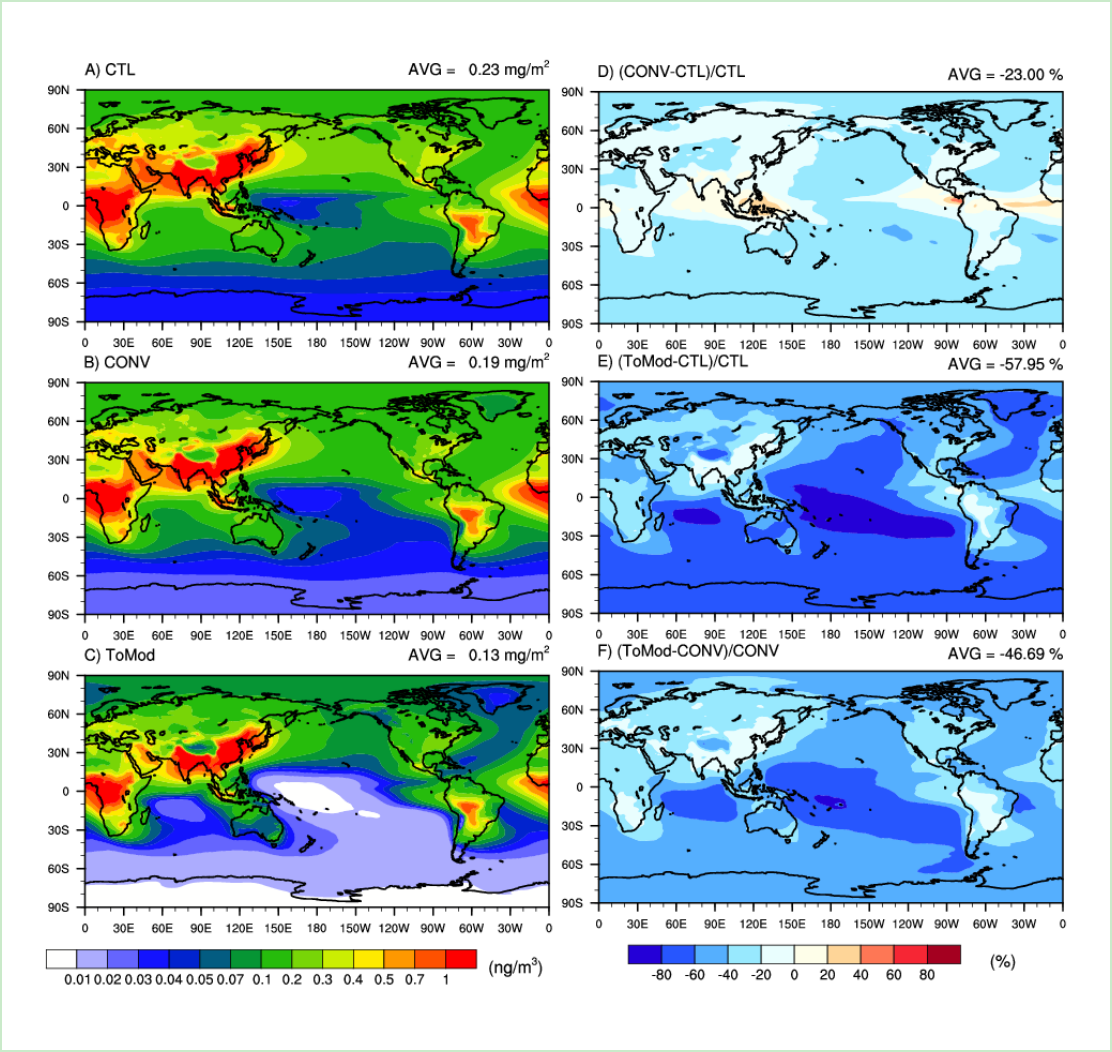

Fig. 2. Same as Fig. 1., but for BC aerosols.

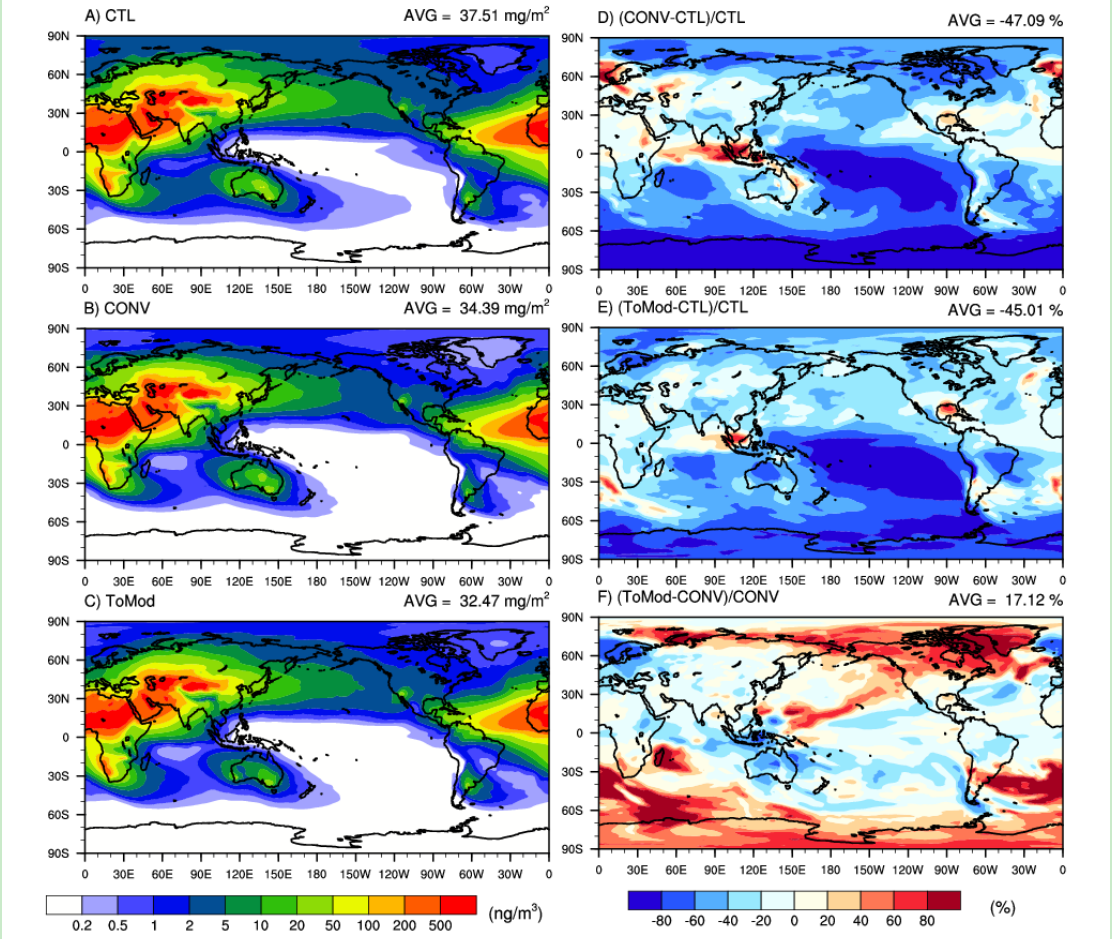

Fig. 3. Same as Fig. 1., but for dust.

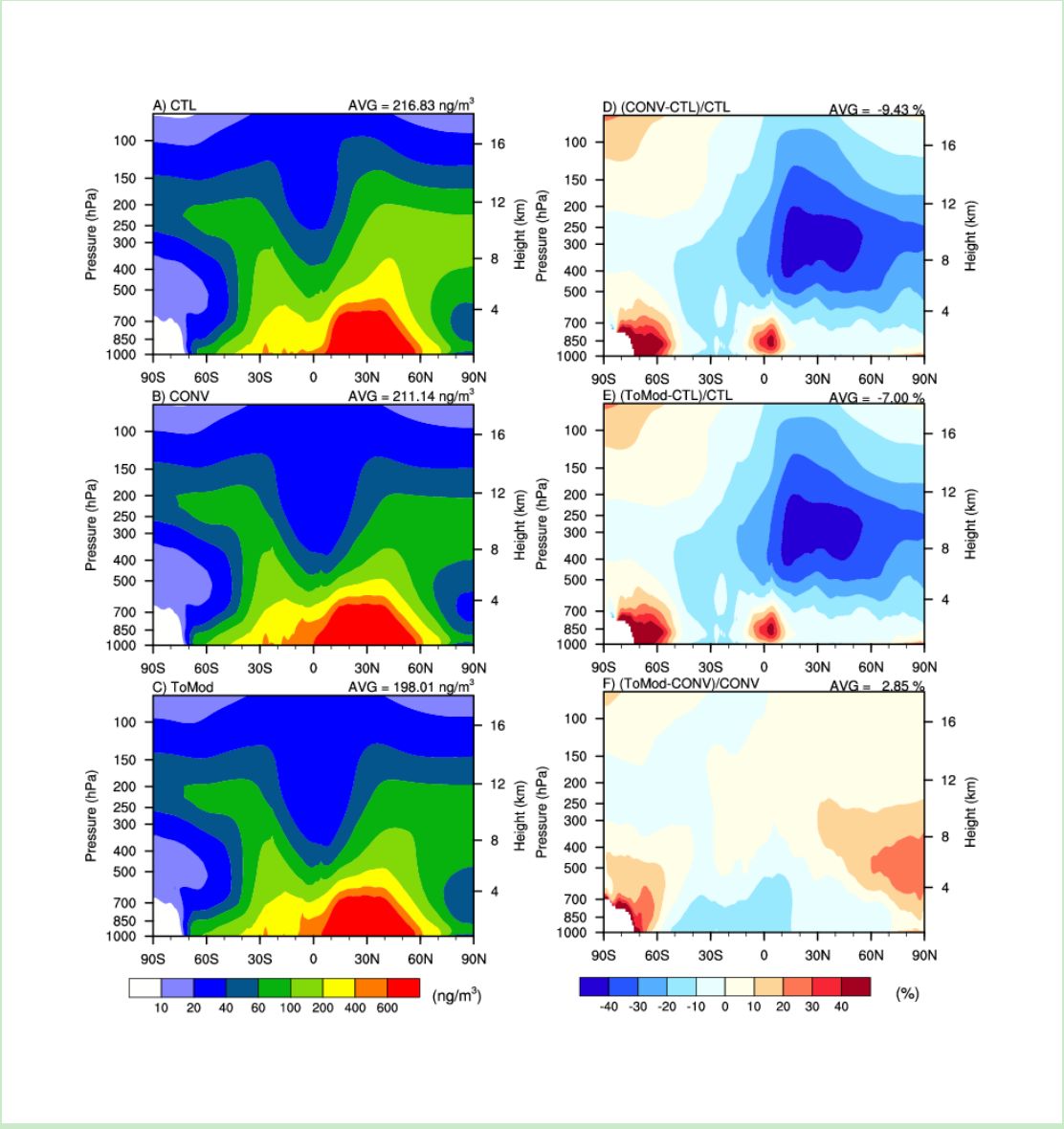

Fig. 4. Zonal distributions of annual mean sulfate aerosols in CTL (a), CONV (b) and ToMod (c). (d), (e) and (f) are relative differences between CTL and CONV, CTL and ToMod, ToMod and CONV. The acronyms are described in Table 1. The numbers on the panels denote the global average.

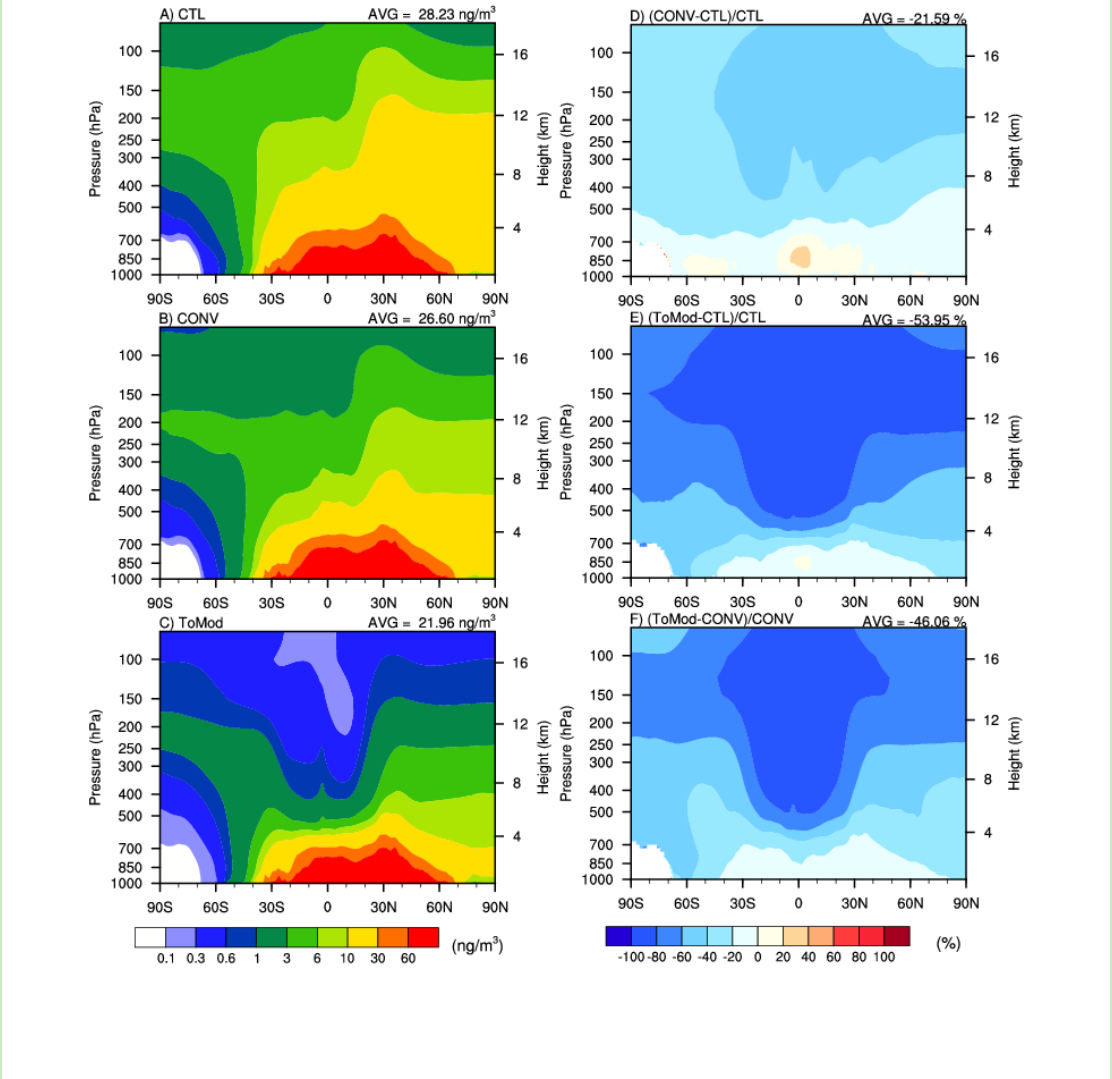

Fig. 5. Same as Fig. 4, but for BC aerosols.

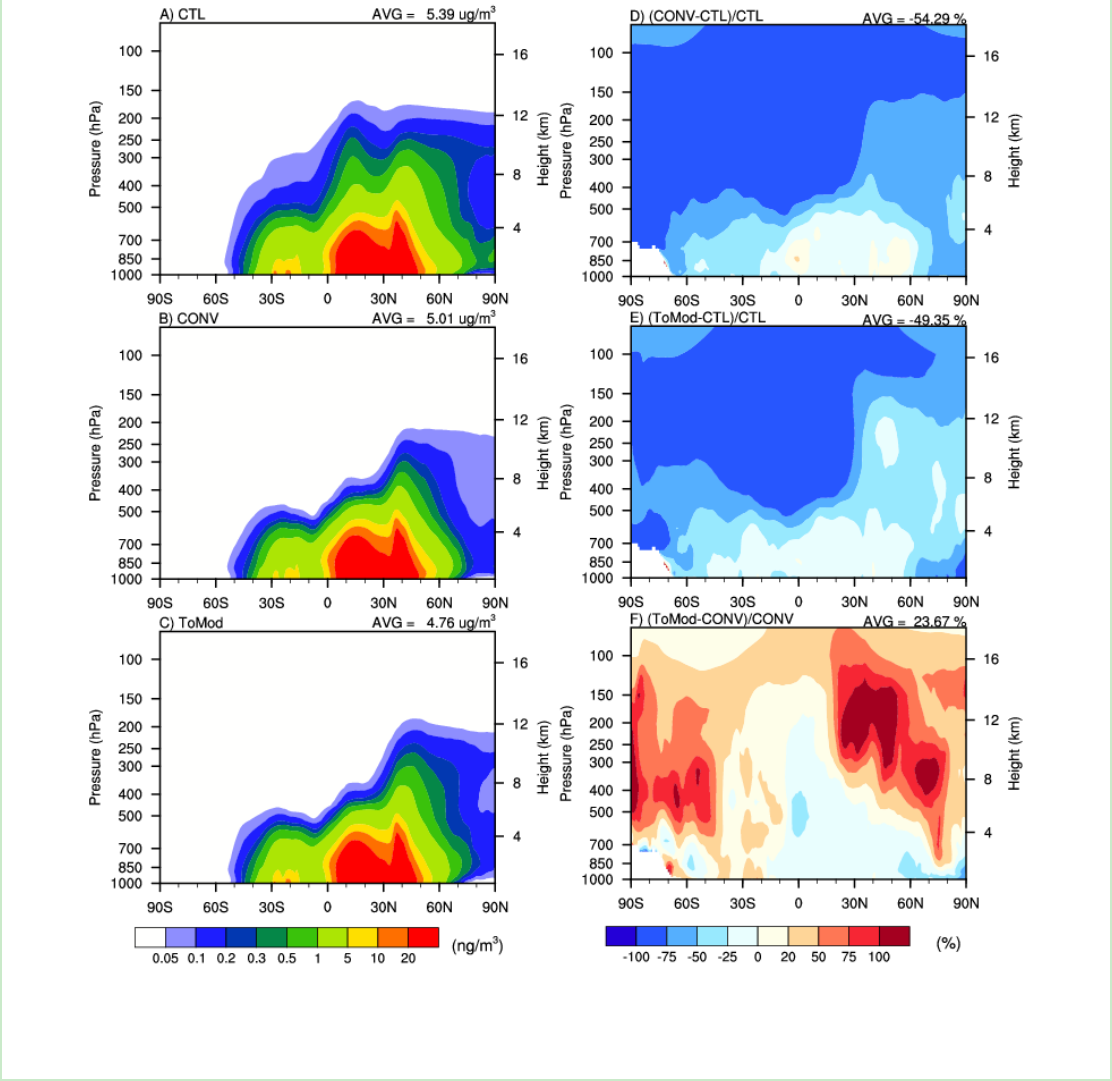

Fig. 6. Same as Fig. 4, but for dust aerosols

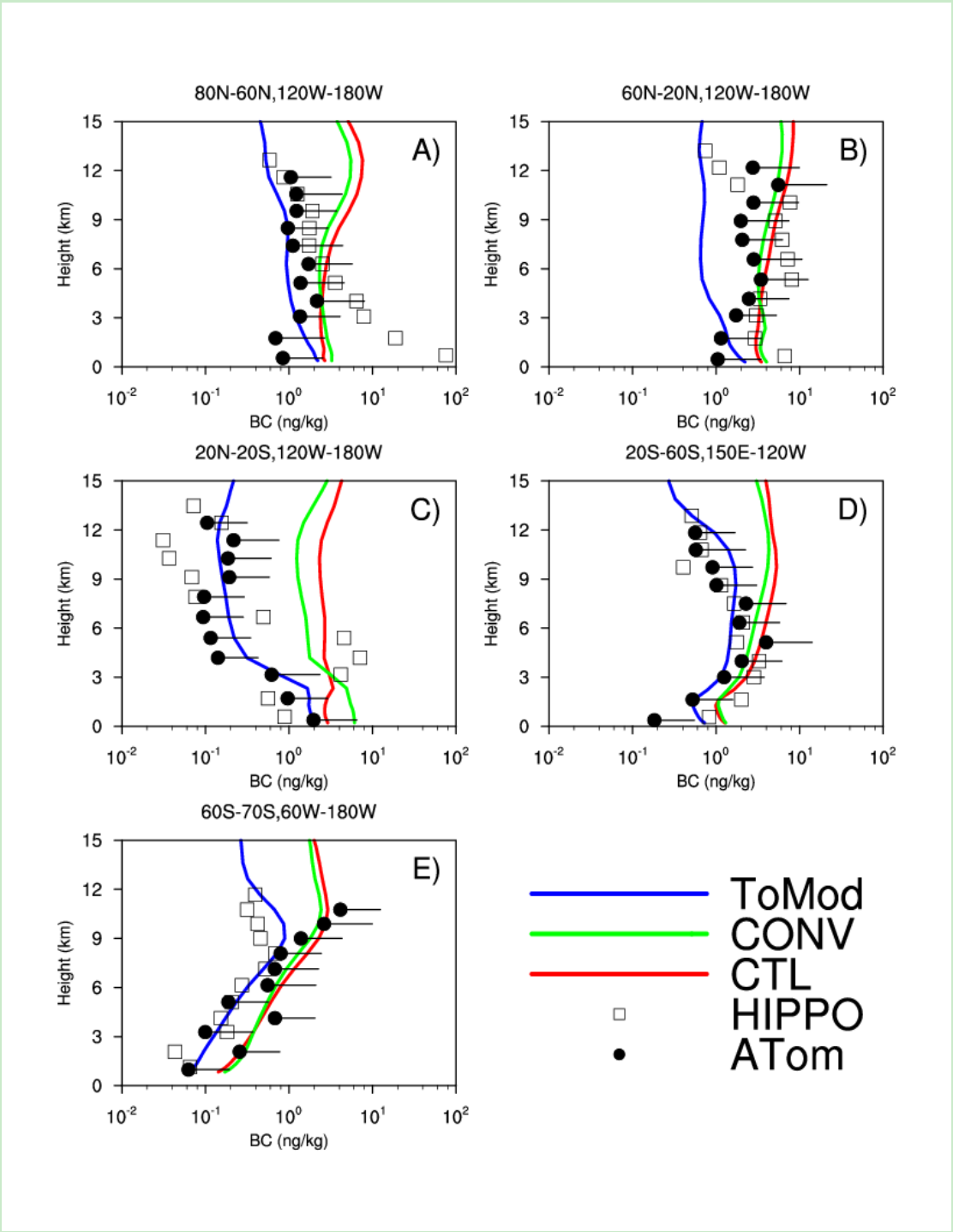

Fig. 7. Vertical profiles of BC mass mixing ratios (ng kg^{-1}) from HIPPO, ATom and model simulations over Pacific Ocean. Profiles from the model output are sampled along flight tracks within the latitude– longitude range for each panel. ATom has four sampling time periods: 07/29/2016 to 08/23/2016, 01/26/2017 to 02/21/2017, 09/28/2017 to 10/26/2017 and 04/24/2018 to 05/21/2018 that roughly represent four seasons. HIPPO has five sampling time periods: 01/08/2009 to 01/30/2009, 10/31/2009 to 11/22/2009, 03/24/2010 to 04/16/2010, 06/14/2011 to 07/14/2011 and 08/09/2011 to 09/09/2011. The acronyms are described in Table 1.

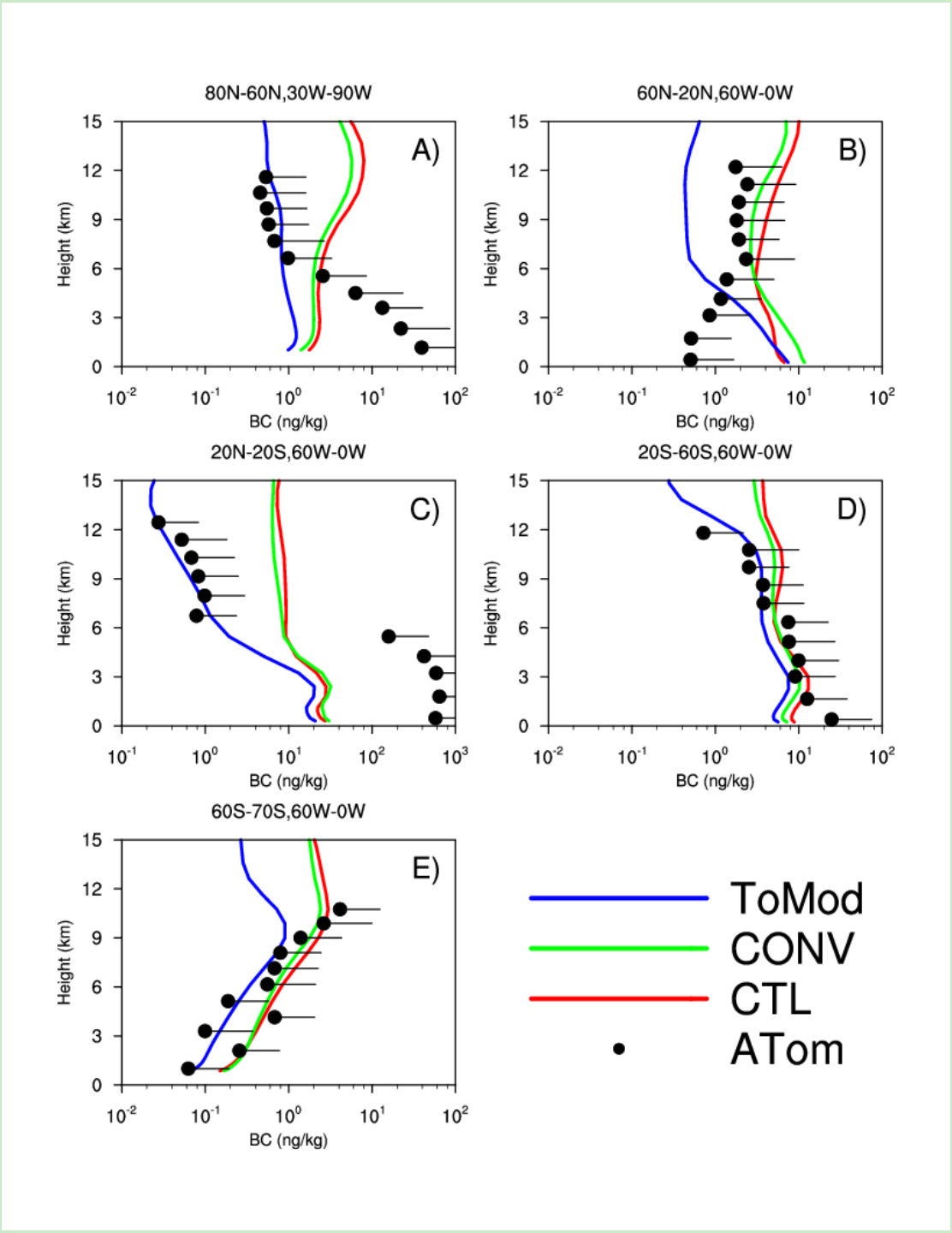

Fig. 8. Same as Fig. 7 but for the BC profiles over the Atlantic Ocean.

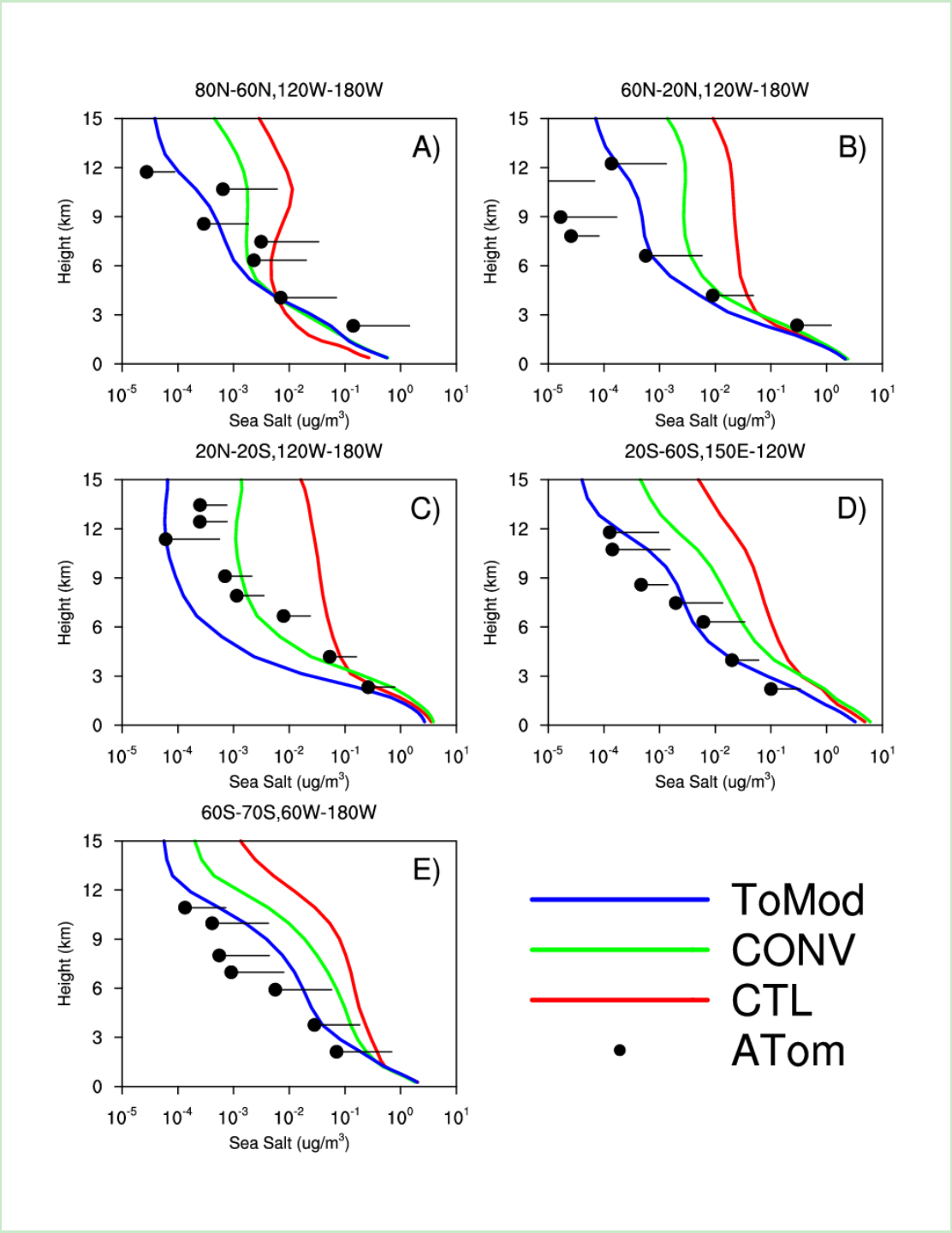

Fig. 9. Vertical profiles of sea salt mass concentration (μg m^{-3}) over Pacific Ocean from ATom and model simulations. Profiles from the model output are sampled along flight tracks within the latitude–longitude range for each panel. The acronyms are described in Table 1.

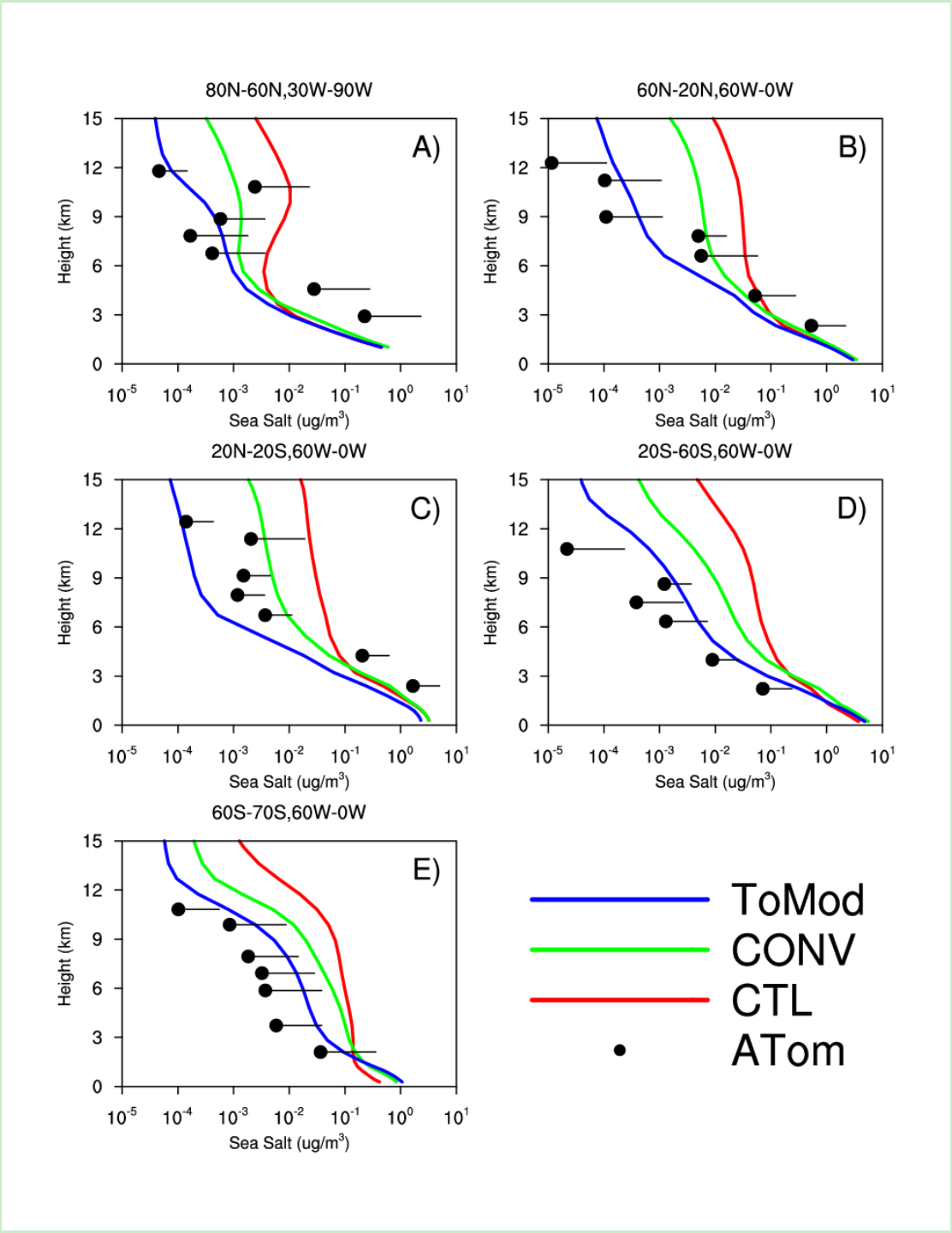

Fig. 10. Same as Fig. 9 but for the sea salt profiles over the Atlantic Ocean.

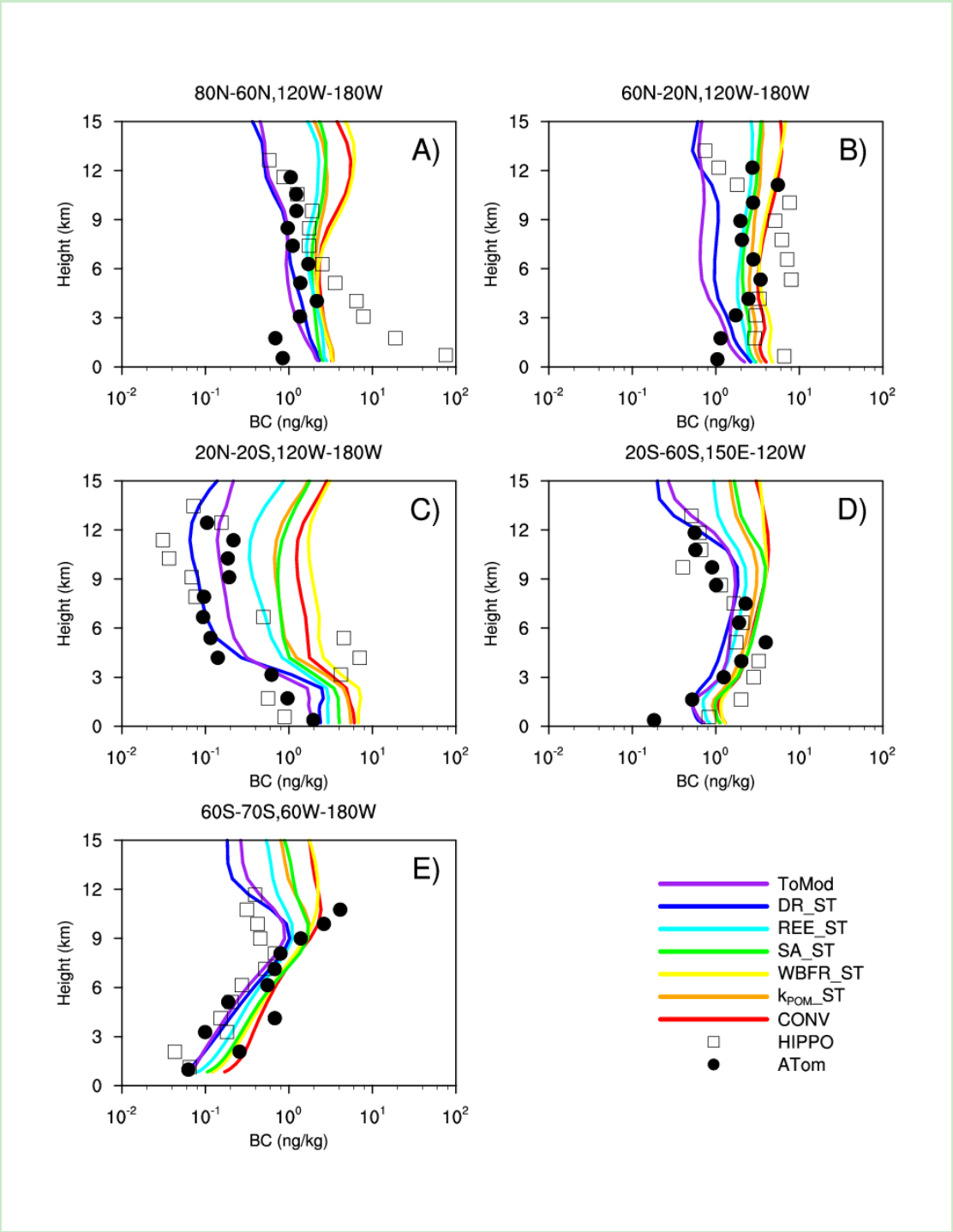

Fig. S1. Vertical profiles of BC mass mixing ratios (ng kg^{-1}) from HIPPO, ATom and model simulations over Pacific Ocean, where the simulations involve CONV, WBFR, SA, REE, DR and ToMod (see explicit statements in Table 1). Profiles from the model output are sampled along flight tracks within the latitude–longitude range for each panel. The acronyms are described in Table 1.

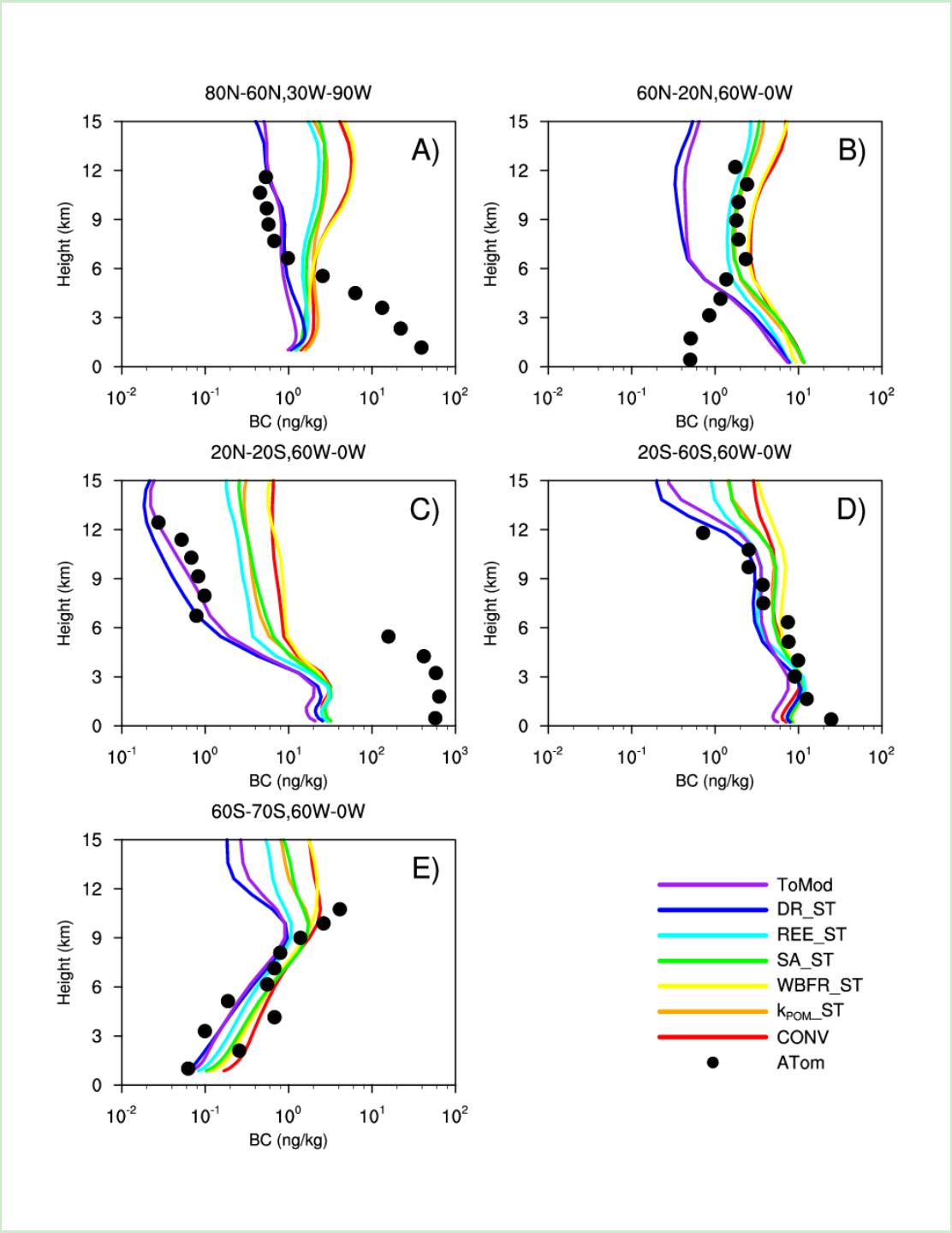

Fig. S2. Same as Fig. S1 but for the BC profiles over the Atlantic Ocean.

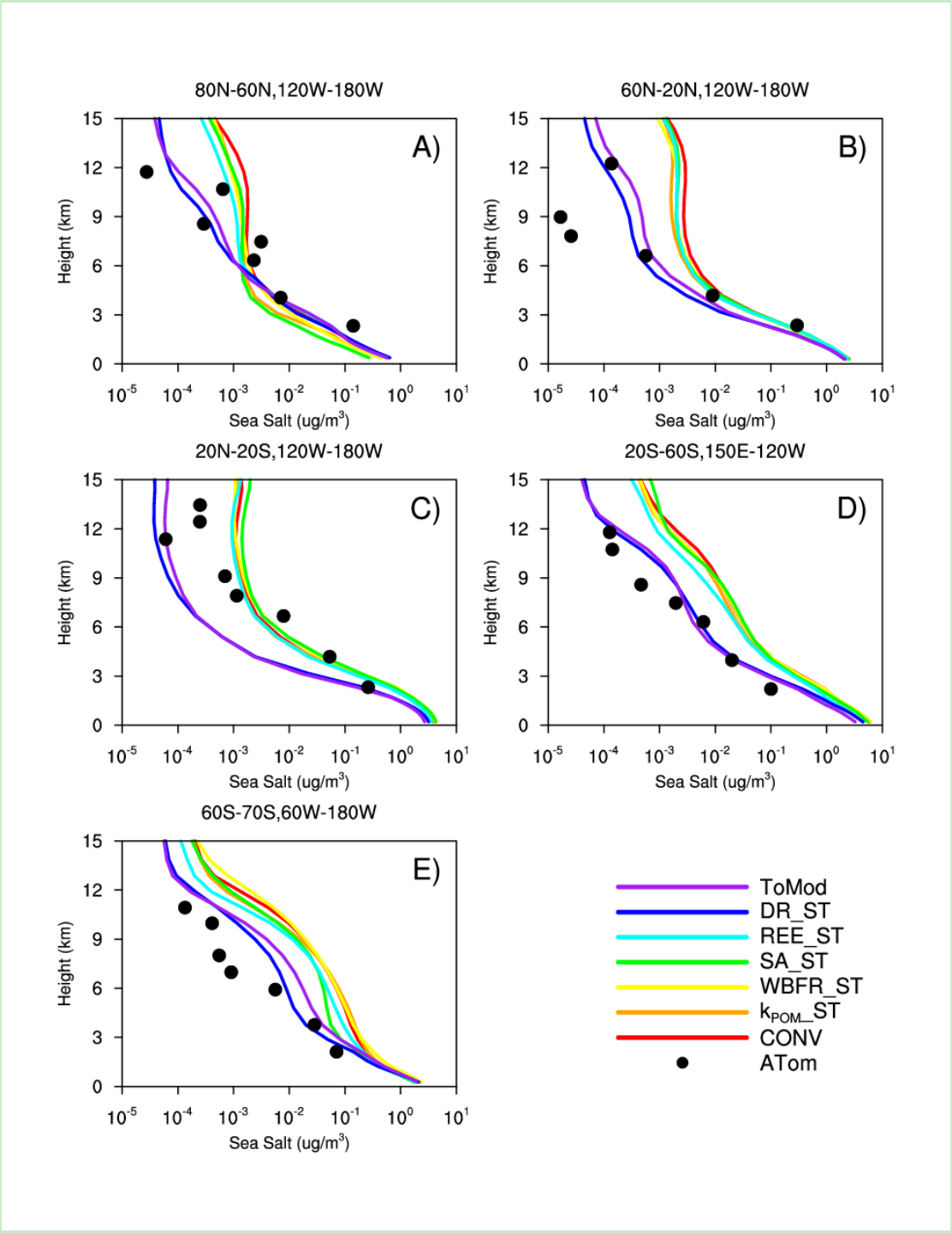

Fig. S3. Same as Fig. S1 but for the sea salt profiles over the Pacific Ocean.

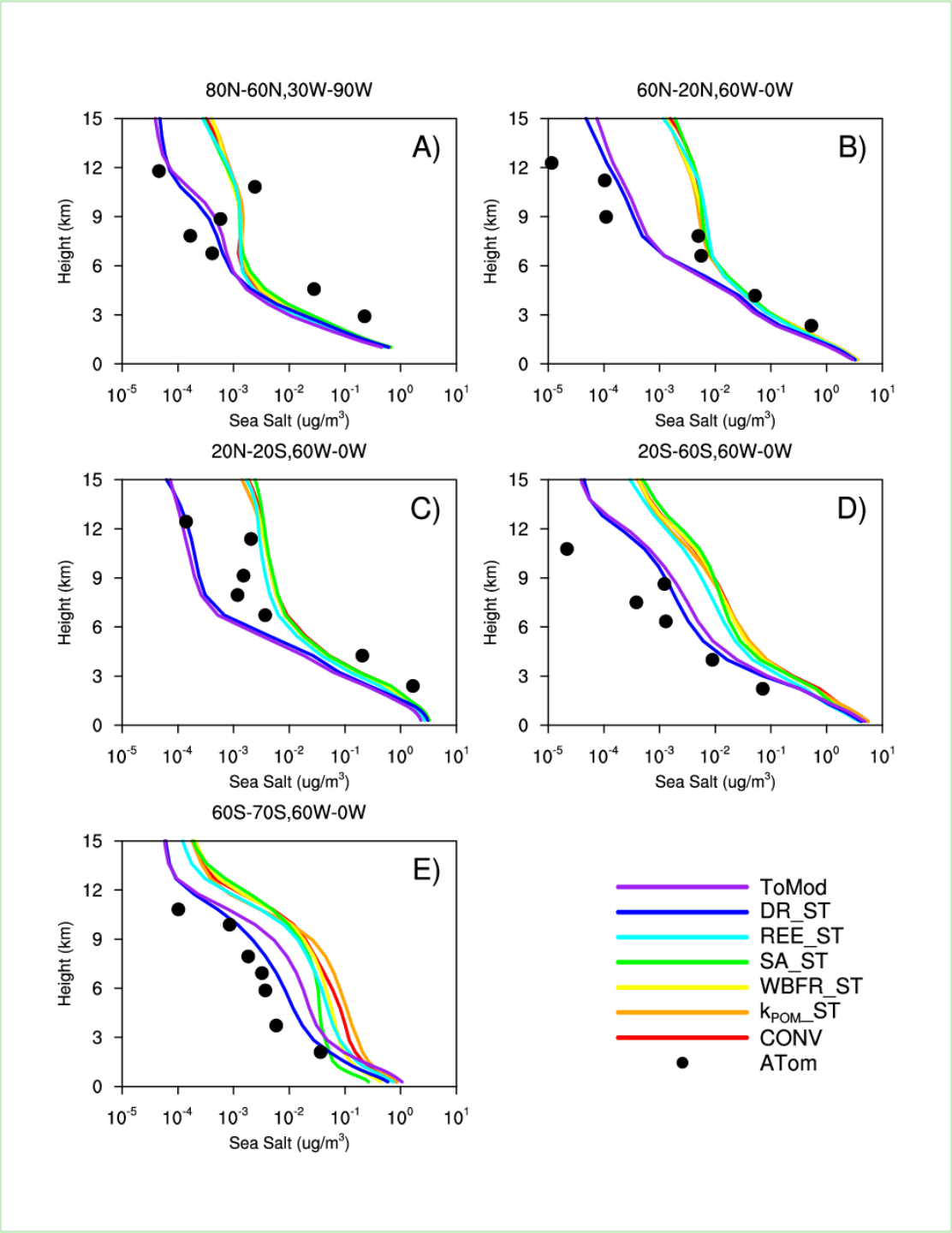

Fig. S4. Same as Fig. S1 but for the sea salt profiles over the Atlantic Ocean.

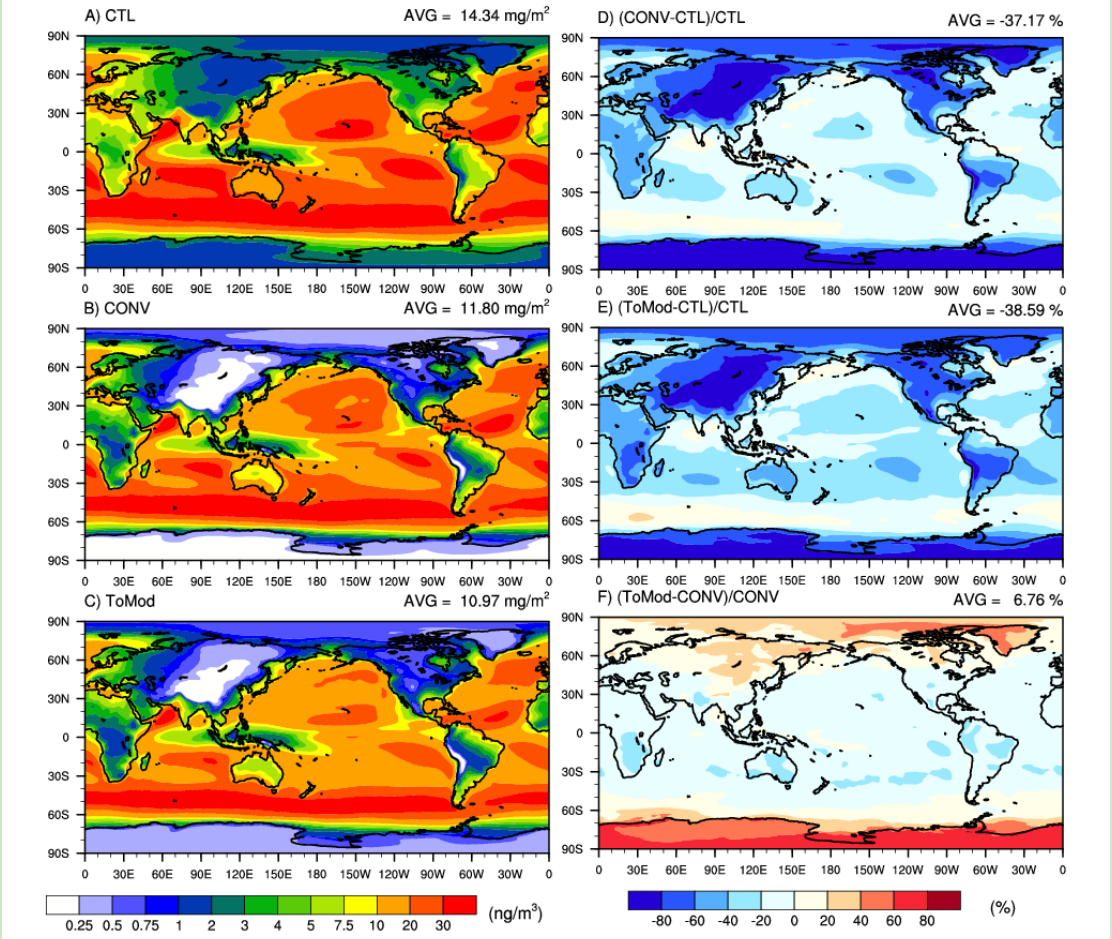

Fig. S5. Same as Fig. 1, but for sea salt.

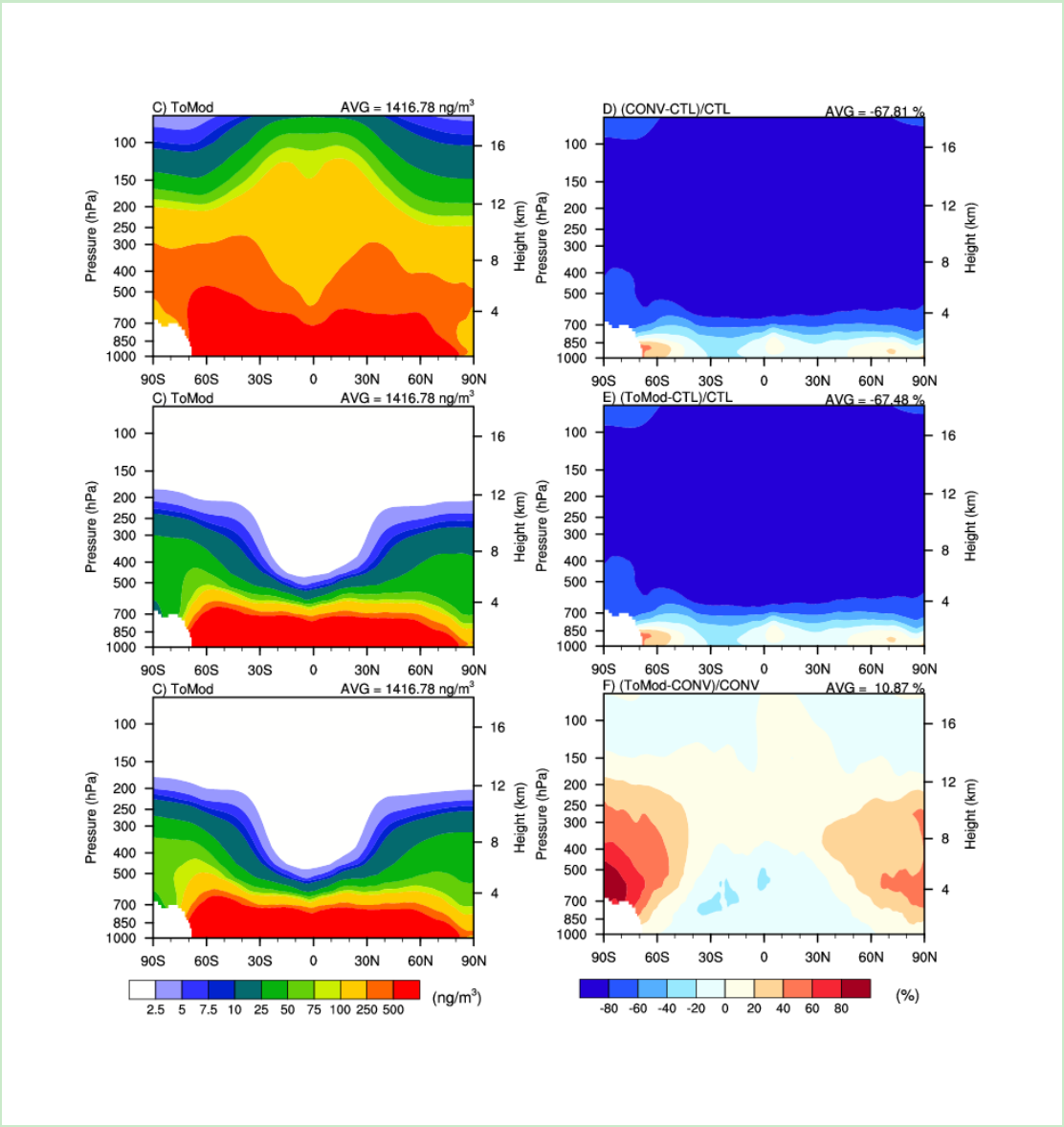

Fig. S6. Same as Fig. 4, but for sea salt aerosols.